NASA Technical Paper 2222

October 1984

Flight-Determined Aerodynamic Derivatives of the AD-1 Oblique-Wing Research Airplane

Alex G. Sim
and Robert E. Curry

NASA

NASA Technical Paper 2222

1984

Flight-Determined Aerodynamic Derivatives of the AD-1 Oblique-Wing Research Airplane

Alex G. Sim
and Robert E. Curry

NASA Ames Research Center
Dryden Flight Research Facility
Edwards, California

National Aeronautics
and Space Administration

Scientific and Technical Information Branch

INTRODUCTION

Studies of the oblique-wing concept have shown substantially improved transonic aerodynamic performance at Mach numbers up to 1.4, and flight without sonic booms at Mach numbers as high as 1.2 (ref. 1). Subsonic oblique-wing transport studies (ref. 2) have shown the potential for either increased range or reduced takeoff gross weight. Common to the configurations of both studies is the inherently low airport noise and generally better low-speed performance characteristics. An overview of oblique-wing applications is presented in reference 3. Although oblique-wing aerodynamic performance benefits occur at transonic speeds, many of the problems associated with asymmetry are not strongly tied to compressibility and thus, to a limited extent, can be studied at low speeds.

The AD-1 airplane was designed and fabricated to be a low-speed, low-cost airplane with which research could be conducted on many of the problems associated with an aeroelastic oblique-wing airplane. The "low cost, low speed" concept limited both the complexity of the vehicle and the scope of the technical objectives. Low speed allowed the use of a low-technology structure, fixed landing gear, and mechanical control system. Technical objectives were limited by the use of a minimal 40-channel instrumentation system. The specific technical objectives of the AD-1 program were (1) assessment of the unique handling and flying qualities of an unaugmented, low-speed, oblique-wing vehicle; (2) general appraisal of the nature and complexity of a flight control system on an oblique-wing configuration; (3) verification of the wing static aeroelastic design criteria; and (4) comparison of the flight-determined aerodynamic data with predictions.

The geometric configuration of the AD-1 airplane was selected from airplane configurations studied by the Boeing Commercial Airplane Company under contract to NASA (ref. 1). While the overall vehicle design was specified by NASA, the detailed design and load analyses were conducted under a contracted effort by the Rutan Aircraft Factory. The airplane was fabricated under a contracted effort by the Ames Industrial Corporation.

In this report, the flight-determined derivatives are compared with predictions. A final "best estimate" of the derivatives is also presented. The derivatives presented were used to document the vehicle's unique aerodynamic characteristics, to analyze the total forces and moments (ref. 4), and to update the real-time simulation for flight planning and safety of flight.

NOMENCLATURE

The right-hand rule is used as a basis for the force and moment sign convention, and all coefficients and derivatives are referenced to the body axes. All data are referenced to a longitudinal center of gravity at the wing pivot (that is, c.g. = $0.4c_r$), are for the right wingtip forward or at zero sweep, and include the effects of landing gear. Wing sweep is the sweep angle of the straight chord line on the wing. For the flight vehicle, the straight chord line of the wing is at approximately 27 percent. For the wind tunnel tests, wings with straight quarter chord, 30-percent chord, and mid chord were used.

b	reference and actual unswept wingspan, m (ft)
c.g.	center of gravity, fraction of c_r
c_r	reference and unswept wing root chord, m (ft)
g	acceleration due to gravity, g
I_x	rolling moment of inertia, kg-m^2 (slug-ft^2)
I_{xy}	x-y cross product of inertia, kg-m^2 (slug-ft^2)
I_{xz}	x-z cross product of inertia, kg-m^2 (slug-ft^2)
I_y	pitching moment of inertia, kg-m^2 (slug-ft^2)
I_z	yawing moment of inertia, kg-m^2 (slug-ft^2)
p	roll rate, deg/sec or rad/sec
q	pitch rate, deg/sec or rad/sec
r	yaw rate, deg/sec or rad/sec
V	velocity, m/sec (ft/sec)
α	angle of attack, deg
β	angle of sideslip, deg
δ_a	aileron deflection, $\delta_{a_{left}} - \delta_{a_{right}}$, deg
δ_e	elevator deflection, deg
δ_r	rudder deflection, deg
η	fraction of semispan
Λ	wing sweep angle, deg

Coefficients:

C_ℓ	rolling moment
C_m	pitching moment
C_N	normal force
C_n	yawing moment
C_Y	sideforce

Derivatives:

$$C_{m_i} = \frac{\partial C_m}{\partial i}, \text{ per deg}$$

$$C_{m_j} = \frac{\partial C_m}{\partial \frac{jc_r}{2V}}, \text{ per rad}$$

$$C_{m_k} = \frac{\partial C_m}{\partial \frac{kb}{2V}}, \text{ per rad}$$

where

$i = g, \alpha, \beta, \delta_a, \delta_e, \delta_r$

$j = q, \dot{\alpha}$

$k = p, r, \dot{\beta}$

Derivatives with respect to C_ℓ, C_N, C_n, and C_Y are similar to those for C_m.

VEHICLE DESCRIPTION

The general layout of the AD-1 airplane, shown in figure 1, consists of a high-fineness-ratio fuselage, two turbojet engines mounted on short pylons on the side of the fuselage, fixed gear, and a high-aspect-ratio aeroelastic variable-sweep oblique wing. A total fuel capacity of 270 liters (72 gal) is stored in two fuselage tanks located forward and aft of the wing pivot location. For these tests, the flight c.g. was generally within a few percent of its nominal quarter root chord value. Additional physical characteristics are given in table 1.

Structurally, the airplane consists of a fiberglass-reinforced plastic sandwich separated by a core of rigid foam. Except for the wing pivot, all structural components were designed to a 6g limit load capability and a 175-KEAS limit airspeed. The wing pivot was designed to a load limit of ±25g.

The primary flight controls were conventional aileron, elevator, and rudder, which were actuated using a mechanical control system. The rudder pedals were mechanically linked to the upper rudder; yaw trim was provided by the electrically operated lower rudder. Pitch and roll trim were obtained from electrically operated tabs located on the elevator and right aileron, respectively. Wing sweep was initiated using a switch on the instrument panel. The wing could be returned to the unswept position using either the switch or a trigger on the pilot's center stick. The wing could only be swept in one direction, with the right wingtip sweeping forward.

An 8-bit, 40-channel, 200-sample-per-second (sps) instrumentation system was used to provide flight data. Consistent with the low-cost concept, the instrumentation system was the minimum required to both accomplish the technical objectives and ensure safety of flight. A list of instrumentation parameters relevant to the aerodynamic data analysis is presented in table 2.

Ground vibration, structural loading, and moment of inertia tests were conducted prior to the first flight. The moments of inertia are of primary interest and are presented in table 3.

PREDICTED DATA

The primary source of the predictions was wind tunnel data. However, computational analyses were used to obtain the damping and rudder derivatives, and are discussed with those parameters.

Wind Tunnel Tests

Wind tunnel testing for the AD-1 configurations was conducted in the NASA Ames 12-Foot Pressure Wind Tunnel using an aeroelastic 1/6-scale model. Full-scale Reynolds number as well as full-scale wing flexibility were obtained when operating at 4.5 atmospheres and Mach 0.3. While most of the data were obtained at these conditions, limited data were also obtained at lower Mach numbers or tunnel pressures to obtain vehicle characteristics at higher angles of attack or off-nominal wing flexibility. Most of the wind tunnel data were obtained over an angle-of-attack range from -4° to 11°. Except where noted, predictions outside this range are based on an extrapolated fairing of the wind tunnel data. The predictions presented have been digitized every 4° angle of attack. The wind tunnel data were obtained at wing sweeps of 0°, 25°, 45°, and 60°. These data were interpolated to obtain predictions at 15° and 30°.

The first wind tunnel tests were conducted with a bottom-mounted blade support (fig. 2) and a straight midchord aluminum wing. Although these tests produced a reasonably complete set of wind tunnel data, the results were unrealistic because of apparent losses in elevator control effectiveness accompanied by a 30-percent increase in static margin. These anomalies brought about a second set of tests which, through flow visualization studies and a model component buildup, revealed that the bottom-mounted blade model support was producing aerodynamic interference in the region of the aft fuselage and horizontal tail. Although it was obvious that the interference affected pitching moment, and to a lesser degree rolling moment, its effect on yawing moment was unknown. The problem with pitching and rolling interference was resolved by using a top-mounted blade support system, also shown in figure 2. However, as was expected, the top-mounted blade support interfered with the vertical tail, necessitating the use of data from the bottom-mounted support system to define yawing moment, sideslip, and rudder characteristics.

From the detailed actual airplane design, it was determined that a fiberglass wing could not be fabricated practically with the scaled stiffness of the original model's straight midchord aluminum wing. Two new model wings were machined out of solid bars of fiberglass to achieve the same scaled stiffness as in the detailed design of the airplane (about one-third as stiff as the aluminum wing). Slight changes in planform were incorporated in the new wings to compensate for their

increased flexibility. One new wing had a straight 30-percent chord line, while the other had a straight quarter chord line. All three wings had the same aspect ratio, taper ratio, and airfoil. The aeroelastic characteristics of both the straight quarter chord and straight 30-percent chord wings were found to be acceptable.

Forces and Moments

A detailed flight-to-wind-tunnel comparison of the aerodynamic forces, moments, and aeroelastics is presented in reference 4; therefore, only an example of the prediction for the longitudinal static stability derivative, C_{m_α}, is presented herein. The predictions have been adjusted to a 1g flight condition.

Sideslip Characteristics

As stated previously, it was necessary to use the bottom-mounted blade support to obtain sideslip characteristics. The wind tunnel tests consisted of sideslip variations of ±5° at constant angles of attack for each wing sweep. No aeroelastic effects were found. The data for the 0° sweep configuration were linearized about 0° sideslip. For the swept configurations, the data were linearized about -2° sideslip since it was recognized that the airplane would trim at slightly negative angles. Although the sideslip predictions were based on wind tunnel data, predictions for C_{m_β} contained extensive interpretation.

Control Surface Characteristics

The aileron characteristics were obtained from wind tunnel tests of the straight midchord aluminum wing. The other two wings did not have ailerons. Although there were only slight geometric differences between model and flight vehicle geometries, the higher torsional rigidity of the aluminum wing resulted in higher aileron control power. Right and left ailerons were tested separately, both up and down, using 8.1° of deflection. Minor left-to-right asymmetries were shown to exist in the wind tunnel results; however, to compare with flight, these effects were averaged to form combined aileron derivatives. For the pitching moment due to aileron parameter, $C_{m_{\delta_a}}$, wind tunnel results were not consistent and were calculated using the wind tunnel value for $C_{\ell_{\delta_a}}$ and the equation

$$C_{m_{\delta_a}} = -\frac{b}{c_r} C_{\ell_{\delta_a}} \tan \Lambda \qquad (1)$$

Elevator effects were obtained from wind tunnel data at elevator positions of -8°, 0°, 8.5°, and 13.5°. Predictions were linearized around an approximate trimmed flight value.

The initial rudder characteristics (which are not included in this report) were obtained from wind tunnel tests at wing yaw angles of 0° and 45°. Using the bottom-mounted blade support, sideslip sweeps were performed at several constant angles of attack with and without 14.1° of rudder. Only slight variations in the resulting derivatives occurred as a result of wing sweep. Subsequent to the wind tunnel tests, it was decided to change the rudder geometry by both increasing the rudder chord by 20 percent and splitting the control surface at its midwaterline. The new upper rudder was used for pilot control, while the new lower rudder was used for yaw trim.

To estimate the new rudder derivatives, the initial rudder characteristics were computed using the Vortex-Lattice program of reference 5. Next, the scale factor necessary to adjust these computations to the wind tunnel values was determined. Finally, the new rudder geometry was analyzed using the Vortex-Lattice program and was scaled using the previously determined factor. At higher angles of attack, the computed values were decreased to reflect the reduction in C_{n_β} for which higher-angle-of-attack wind tunnel data were available.

Damping Characteristics

The primary tool for estimating damping derivatives was the STBDER computer program of reference 6. Its primary application is to compute static and dynamic derivatives for oblique-wing vehicles in the subsonic flight regime. STBDER uses lifting line theory for the wing contribution, and classical methods for the remaining vehicle components. Using the program, the straight taper wing of the AD-1 vehicle was approximated with a rigid straight quarter chord, elliptically tapered wing. The correlation between flight and STBDER damping derivatives has previously been shown to be good (ref. 7). As an additional check, the Vortex-Lattice program of reference 5 was used to compute several of the primary damping derivatives at 0° and 45° wing sweep.

Damping derivatives obtained from references 5 and 6 are purely rotary derivatives and are not combined with the translational acceleration derivatives. Generally, damping derivatives obtained from either flight or oscillatory wind tunnel tests combine the rotary and translational acceleration derivatives into a single damping parameter. As an example, C_{m_q} and $C_{m_{\dot{\alpha}}}$ are combined to form the parameter $C_{m_q} + C_{m_{\dot{\alpha}}}$. It is common practice to call this parameter only by its rotary derivative name, C_{m_q}. All flight derivatives in this report are called only by their rotary derivative names. Reference 8 gives an example of a flight analysis where the rotary and translational acceleration derivatives were separated. When computing damping derivatives, the translational acceleration derivatives are often neglected because most of them are relatively small and because techniques to compute them are not readily available. However, the translational acceleration derivatives $C_{m_{\dot{\alpha}}}$ and $C_{n_{\dot{\beta}}}$ are often significant; thus the predictions for C_{m_q} and C_{n_r} are probably low because they underestimate the damping parameters $C_{m_q} + C_{m_{\dot{\alpha}}}$ and $C_{n_r} + C_{n_{\dot{\beta}}}$, respectively.

FLIGHT DERIVATIVE ANALYSIS

The MMLE3 program (ref. 9), which is one of the most widely accepted and best techniques for estimating stability and control derivatives, was the primary flight data analysis tool. MMLE3 uses a maximum likelihood estimation method of analysis. The program is user friendly, allowing for rapid software modification (ref. 10), and has aircraft-specific subroutines that allow most of the input to be defaulted.

For the AD-1 analysis, the program was modified to include an aerodynamic model similar to the model used in reference 7. This model separated the longitudinal and lateral-directional equations of motion but included the effects of the aerodynamic

cross-coupling terms. This was done in the longitudinal analysis by eliminating the differential equations for the lateral-directional motion and using measured lateral-directional responses as inputs to the longitudinal equations. Similarly, the lateral-directional analysis uses the measured longitudinal responses. The effects of the cross product of inertia, I_{xy}, were included. Unlike the model of reference 7, the engine gyroscopic effects were not included. Neither model included the aeroelastic effects.

When using MMLE3, a measure of the accuracy of each derivative is provided in the form of Cramér-Rao bounds. An evaluation of the use and accuracy of the Cramér-Rao bounds is given in reference 11. To accentuate the bounds on the plotted results, they were multiplied by a scale factor of 2. The large Cramér-Rao bounds (low derivative accuracy) have been attributed to many types of problems, including aerodynamic modeling inaccuracies such as when nonlinear terms are not modeled, external inputs such as turbulence that is not modeled, poorly conditioned maneuvers that exhibit an overdamped response, or a maneuver that is simply too small for the system signal noise. In a flight environment, maneuvers nearly always suffer from one or more of these problems. Thus, it is not unreasonable to sometimes obtain large Cramér-Rao bounds. In addition, some vehicle derivatives have very little effect on vehicle motion and will normally yield poor derivative estimates.

All data maneuvers were performed at an altitude of 3800 m (12,500 ft) and with a load factor of 1. Neglecting slight changes in gross weight, angle of attack could not be varied independent of airspeed. At the higher angles of attack (lower airspeed), the airspeed measurement becomes less accurate, which causes all the derivative estimates to deteriorate. Specific flight maneuvers were performed for MMLE3 analysis. These consisted of a series of doublet control inputs separated by 5 to 7 sec of no control input. Longitudinal maneuvers consisted of two elevator doublets; lateral-directional maneuvers consisted of two rudder doublets followed by two aileron doublets. Aileron doublets were performed last to minimize changes in flight conditions. The longitudinal maneuvers typically lasted 15 sec and were analyzed at 50 sps. Lateral-directional maneuvers, lasting about 30 sec, were analyzed at 25 sps.

As a means of verifying the MMLE3 analysis, a more classic technique (used in ref. 4) was used to compute changes in the forces and moments due to slow sideslip variations. From these maneuvers, linearity in the sideslip characteristics was confirmed, and sideslip derivatives were computed. Although the intent of the maneuvers was to slowly vary sideslip over a $\pm 10°$ range, at higher wing sweeps the vehicle dynamics made it difficult to perform steady maneuvers.

RESULTS AND DISCUSSION

Although a complete set of both longitudinal and lateral-directional derivatives were obtained from flight data, some of the results are not presented herein. Derivatives that describe the total force or moment as a function of angle of attack have been omitted since similar data are presented in reference 4. Derivatives with larger Cramér-Rao bounds have also been omitted. The size of the maximum allowable Cramér-Rao bound for each derivative is presented in table 4. When the Cramér-Rao bound was less than the symbol size, the bound was omitted from the plot.

Longitudinal Flight Results

Consistent MMLE3 longitudinal results were obtained for some of the primary derivatives. For the remaining longitudinal derivatives, consistent results were difficult to obtain. There were three primary reasons for this problem: First, the low-cost considerations for the instrumentation tended to limit the quality of the basic time-response data. Second, the longitudinal response was heavily damped. Third, with the AD-1 aircraft, significant aeroelastic effects and nonlinearities are present that are not modeled in MMLE3.

As shown by both the predictions and the flight results of reference 4, the aeroelastics can be modeled as a change in aircraft moments due to load factor. As an example, the change in pitching moment with load factor is shown in figure 3. Although the data of figure 3 are not linear, they can be linearized over a small incremental range of load factor to yield the linear derivative C_{m_g}. Since C_{m_g} was not modeled, the MMLE3 results should indicate a bias in C_{m_α} — that is, the flight results for C_{m_α} would actually represent a parameter C_{m_α} plus the term C_{m_g}. For this report, the computation of C_{m_α} was not necessary because the reference 4 computation of C_m as a function of α (fig. 4) eliminates the need to use the MMLE3 C_{m_α} value. Figure 4 also illustrates the nonlinearities in the pitching moment curves — especially at angles of attack above 6°. When MMLE3 is modeled with a linear set of derivatives (as it was for the AD-1 aircraft), the derivatives tend to be averaged over the maneuver's incremental angle of attack. This often requires some interpretation of the final results, but it is usually not a major problem by itself.

None of the three problems discussed is considered major by itself. However, the occurrence of all the problems at once can significantly impact the flight data results, as illustrated by C_{m_α} and C_{m_q} (fig. 5). The data exhibit considerable scatter, especially at higher wing sweeps and angles of attack. There is the expected bias in the C_{m_α} results due to the C_{m_g} derivative; however, there is also an unexpected bias in the flight data for C_{m_q} that was discovered when a fairing of the flight data was mechanized in the real-time simulation. Inconsistent data were also obtained for C_{m_β}, C_{m_p}, and C_{m_r}. Indications are that these damping and stability derivatives were often traded, resulting in high levels of scatter and unknown biases in the flight data.

The MMLE3 flight-determined values for C_{m_q} at zero sweep and for $C_{m_{\delta_e}}$ are presented in figure 6. The flight value for the pitch damping derivative, C_{m_q}, is significantly higher than the prediction. Part of this discrepancy is considered to be due to neglecting $C_{m_{\dot{\alpha}}}$, which would have added approximately -4 per radian units to the prediction. Flight values for the pitch control derivative, $C_{m_{\delta_e}}$, are only slightly lower than the predictions. The slight reduction in predicted control power is probably because the control surface is sealed on the wind tunnel model and not on the airplane.

Flight values for C_{m_β}, as computed from sideslip variation maneuvers, are presented in figure 7. The flight data generally verify the predictions although, as previously stated, the C_{m_β} predictions are based on wind tunnel data with significant interpretation.

Lateral-Directional Flight Results

The lateral-directional sideslip derivatives, C_{ℓ_β}, C_{n_β}, and C_{Y_β}, as obtained from the MMLE3 analysis, are presented in figure 8. The figure reveals discrepancies between the flight data and the predictions. The significantly higher values for the predictions are considered to be a result of using the bottom-mounted blade support. A more interesting effect is the decrease in C_{n_β} with wing sweep at the higher angles of attack. Because C_{Y_β} does not decrease with wing sweep and only slightly decreases with angle of attack, the decreases in C_{n_β} with sweep are considered to be a wing effect. Because the flight c.g. was about 15-percent c_r forward of this report's reference c.g., flight values for C_{n_β} were about 0.00022 more positive (that is, more stable) than the data shown in figure 8. The effective dihedral derivative, C_{ℓ_β}, increases with sweep at higher wing sweeps and angles of attack. The physical reasons for the high-angle-of-attack changes in C_{ℓ_β} and C_{n_β} with wing sweep are not understood. The sideslip derivatives obtained from sideslip variation maneuvers are presented in figure 9 and are shown to verify the MMLE3 results.

The aileron control derivatives, $C_{\ell_{\delta_a}}$, $C_{n_{\delta_a}}$, and $C_{Y_{\delta_a}}$, are plotted in figure 10 as functions of angle of attack and in figure 11 as functions of wing sweep. The primary aileron control derivative, $C_{\ell_{\delta_a}}$, is shown to decrease with both angle of attack and wing sweep. Although both these trends are consistent with the predictions, the flight values are generally less than the predicted values for sweep angles less than 60°. The probable reason is the lower torsional rigidity of the airplane wing as compared with the aluminum wind tunnel model wing. Control authority at the higher sweep angles was low but was satisfactory since the ailerons were originally designed to provide adequate control at 60° wing sweep. As the wing is swept, roll damping and roll inertia also decrease.

Yawing moment due to aileron, $C_{n_{\delta_a}}$, becomes more proverse as angle of attack is increased and more adverse as wing sweep is increased. At the lower wing sweeps, $C_{n_{\delta_a}}$ is small relative to $C_{\ell_{\delta_a}}$ and thus not a major influence on the vehicle's handling qualities. Near 60° sweep at lower angles of attack, $C_{n_{\delta_a}}$, relative to $C_{\ell_{\delta_a}}$, is large enough to cause some undesirable adverse yaw. The sideforce due to aileron, $C_{Y_{\delta_a}}$, is a derivative with little influence on the vehicle response. Thus, the flight values are poorly defined, leaving the predictions as the best estimate.

The rudder control derivatives, $C_{\ell_{\delta_r}}$, $C_{n_{\delta_r}}$, and $C_{Y_{\delta_r}}$, are presented in figure 12 and show reasonable agreement with predictions. There were no discernible variations

with either angle of attack or wing sweep. Yaw control authority was generally adequate to maneuver and fly the vehicle. However, to either trim the vehicle with wing sweeps approaching 60° or to attain high sideslip angles for the sideslip variation maneuvers, the rudder trim surface's control authority was needed.

The roll damping derivatives, C_{ℓ_q}, C_{ℓ_p}, and C_{ℓ_r}, are plotted as functions of angle of attack in figure 13 and as functions of wing sweep in figure 14. The damping in roll due to pitch rate derivative, C_{ℓ_q}, contains considerable scatter. Of the lateral-directional derivatives, both C_{ℓ_q} and C_{n_q} (not yet presented) are in error because the engine gyroscopic effect was not modeled. The error is on the order of 20 percent, whereas the scatter is over 100 percent. Since these derivatives cross into the pitch axis, they were degraded by many of the same problems encountered with the longitudinal analysis; therefore, the prediction is the best estimate for C_{ℓ_q}. The primary roll damping parameter, C_{ℓ_p}, decreases (becomes less negative) with both wing sweep and angle of attack. The apparent scatter around 15° sweep is from maneuvers with higher frequency control inputs that were performed for structural analysis but later analyzed using MMLE3. The large and predicted reduction in C_{ℓ_p} due to sweep had the predicted degrading effect on the handling qualities. The roll due to yaw rate damping parameter, C_{ℓ_r}, generally verified the predictions, although the flight values are higher than predictions at the higher sweeps and angles of attack.

The yaw damping derivatives, C_{n_q}, C_{n_p}, and C_{n_r}, are presented in figure 15 as functions of angle of attack and in figure 16 as functions of wing sweep. The damping in yaw due to pitch rate derivative, C_{n_q}, is not well defined by the flight data, as stated in the discussion of C_{ℓ_q}. The damping in yaw due to roll rate derivative, C_{n_p}, is reasonably well defined by the flight data and significantly more negative than predicted. The primary damping in yaw parameter, C_{n_r}, is more negative than predicted, indicating a higher level of yaw damping. The $C_{n_{\dot{\beta}}}$ derivative was not included in the prediction for C_{n_r} and is probably the reason for the discrepancy.

Derivative Best Estimates

Engineering judgment was used to compile a "best estimate" set of derivatives. These estimates are based on hand-faired flight, wind tunnel, and computational data, and constitute a final set of derivatives. In conjunction with the data of reference 4, these derivatives provide a complete aerodynamics data package.

A best estimate set of longitudinal derivatives is presented in figure 17. The value of C_{m_β} was estimated based on the flight analysis of the slow sideslip maneuvers shown in figure 7. The values shown for C_{N_β}, C_{m_p}, and C_{m_r} are predicted. The zero-sweep value for C_{m_q} is based on MMLE3 analysis. For nonzero wing sweep, C_{m_q} was estimated by adding the computed prediction increment to the zero-sweep flight value. Real-time simulation indicated that the resulting pitch damping was

representative. The value of $C_{m_{\delta_e}}$ is based on MMLE3 results. The ratio between the predicted and flight values for $C_{m_{\delta_e}}$ was used to compute a scale factor which was then used to scale the predictions for the estimate of $C_{N_{\delta_e}}$. The value of $C_{m_{\delta_a}}$ was computed from the MMLE3 flight results for $C_{\ell_{\delta_a}}$ using equation (1). The estimate for $C_{N_{\delta_a}}$ was zero.

The best estimate set of lateral-directional derivatives is presented in figure 18. Estimates for all major derivatives are based on MMLE3 results. Estimates for $C_{Y_{\delta_a}}$, C_{ℓ_q}, and C_{n_q} are based on the predictions.

CONCLUDING REMARKS

A flight investigation was conducted to provide stability and control derivatives for the AD-1 oblique-wing research airplane. A best preflight set of predictions was estimated based on both wind tunnel and computational analysis results. A correlation between the flight-determined derivatives and the preflight predictions was conducted. Of the major derivatives, $C_{\ell_{\delta_a}}$, C_{ℓ_p}, $C_{m_{\delta_e}}$, and the rudder derivatives verified the predictions. Other major derivatives, C_{ℓ_β}, C_{n_β}, C_{Y_β}, C_{m_q}, and C_{n_r}, did not agree with the predictions. Reasons for the disagreement were discussed. Also discussed were problems encountered with the longitudinal flight analysis. A "best estimate" set of derivatives was presented.

Ames Research Center
Dryden Flight Research Facility
National Aeronautics and Space Administration
Edwards, California, April 29, 1982

REFERENCES

1. Boeing Commercial Airplane Company Preliminary Design Department: Oblique Wing Transonic Transport Configuration Development. NASA CR-151928, 1977.

2. Bradley, E. S.: Summary Report — An Analytical Study for Subsonic Oblique Wing Transport Concept. NASA CR-137897, 1976.

3. Nelms, Walter P.: Applications of Oblique-Wing Technology — An Overview. AIAA Paper 76-943, Sept. 1976.

4. Curry, Robert E.; and Sim, Alex G.: AD-1 Total Forces, Moments, and Aeroelastic Characteristics of an Oblique Wing Research Airplane. NASA TP-2224, 1984.

5. Luckring, James M.: Some Recent Applications of the Suction Analogy to Asymmetric Flow Situations. Vortex-Lattice Utilization, NASA SP-405, 1976, pp. 219-236.

6. Fantino, R. E.; Parsons, E. K.; Powell, J. D.; and Shevell, R. S.: Effects of Asymmetry on the Dynamic Stability of Aircraft. NASA CR-142857, 1975.

7. Maine, Richard E.: Aerodynamic Derivatives for an Oblique Wing Aircraft Estimated From Flight Data by Using a Maximum Likelihood Technique. NASA TP-1336, 1978.

8. Maine, Richard E.; and Iliff, Kenneth W.: Maximum Likelihood Estimation of Translational Acceleration Derivatives from Flight Data. AIAA Article No. 78-1342R, J. Aircraft, vol. 16, no. 10, Oct. 1979, pp. 674-679.

9. Maine, Richard E.; and Iliff, Kenneth W.: User's Manual for MMLE3, a General FORTRAN Program for Maximum Likelihood Parameter Estimation. NASA TP-1563, 1980.

10. Maine, Richard E.: Programmer's Manual for MMLE3, a General FORTRAN Program for Maximum Likelihood Parameter Estimation. NASA TP-1690, 1981.

11. Maine, Richard E.; and Iliff, Kenneth W.: The Theory and Practice of Estimating the Accuracy of Dynamic Flight-Determined Coefficients. NASA RP-1077, 1981.

TABLE 1. — PHYSICAL CHARACTERISTICS OF AD-1 AIRPLANE

Total height, m (ft)	2.06 (6.75)
Total length, m (ft)	11.80 (38.80)
Wing (Λ = 0°) —	
Reference and actual planform area, m^2 (ft^2)	8.60 (93.00)
Reference and unswept span, m (ft)	9.80 (32.30)
Reference and unswept chord (root), m (ft)	1.30 (4.28)
Aspect ratio	11.2
Airfoil	NACA 3612-02, 40 (constant)
Dihedral angle, deg	0
Twist, deg	-2
Root incidence angle, deg	2
Quarter chord sweep angle, deg	0
Leading edge sweep angle, deg	2
Average chord, m (ft)	0.88 (2.90)
Wing pivot location	$0.4c_r$
Sweep angle range, deg	0 to 60
Horizontal tail —	
Planform area, m^2 (ft^2)	2.40 (26.00)
Span, m (ft)	2.40 (8.00)
Average chord, m (ft)	1.00 (3.30)
Root chord, m (ft)	1.60 (5.40)
Dihedral angle, deg	0
Incidence angle, deg	0
Leading edge sweep angle, deg	45
Airfoil	NACA 0006
Vertical tail —	
Area (exposed), m^2 (ft^2)	1.30 (14.40)
Span (exposed), m (ft)	1.10 (3.70)
Average chord, m (ft)	1.20 (3.90)
Root chord, m (ft)	1.80 (5.80)
Leading edge sweep angle, deg	43
Airfoil	NACA 0006
Primary control surfaces —	
Aileron hinge line	$0.75c_r$
Aileron span (total), m (ft)	3.70 (12.00)
Aileron area, each, m^2 (ft^2)	0.28 (3.00)
Aileron root station, $\frac{y}{b/2}$	0.62
Aileron root chord, m (ft)	0.20 (0.65)
Aileron range, each, deg	±25
Elevator hinge line sweep angle, deg	0
Elevator area, m^2 (ft^2)	0.46 (5.00)
Elevator average chord, m (ft)	0.19 (0.62)
Elevator root chord, m (ft)	0.23 (0.75)
Elevator range, deg	25° up to 15° down
Rudder hinge line sweep angle, deg	0
Rudder area, m^2 (ft^2)	0.14 (1.51)
Rudder average chord, m (ft)	0.24 (0.77)
Rudder root chord, m (ft)	0.28 (0.91)
Rudder range, deg	±25

TABLE 1. — Concluded

Masses —

Empty weight, N (lb)	6450 (1450)
Useful load, N (lb)	2930 (695)
Fuel load, N (lb)	2110 (475)
Gross weight, N (lb)	9540 (2145)

Powerplant —

Engines	Two TRS-18-046
Sea-level static thrust, each, N (lb)	979 (220)

TABLE 2. — SELECTED INSTRUMENTATION PARAMETERS

Parameter description	Range	Accuracy
Angle of attack, deg	-5 to 20	0.5
Angle of sideslip, deg	-15 to 15	0.5
Airspeed, knots	0 to 200	3.0
Altitude, m (ft)	0 to 6100 (0 to 20,000)	90.0 (300)
Free air reference temperature, °C (°F)	-45 to 65 (-49 to 149)	2.0 (3.6)
Pitch attitude, deg	-30 to 30	0.6
Roll attitude, deg	-30 to 30	0.6
Pitch rate, deg/sec	-60 to 60	0.3
Roll rate, deg/sec	-60 to 60	0.6
Yaw rate, deg/sec	-30 to 30	0.3
Normal acceleration, g	-1 to 4	0.025
Lateral acceleration, g	-0.5 to 0.5	0.005
Longitudinal acceleration, g	-0.5 to 0.5	0.005
Wing sweep angle, deg	0 to 60	0.6
Right aileron, deg	-25 to 25	0.5
Left aileron, deg	-25 to 25	0.5
Elevator, deg	-27 to 15	0.4
Rudder, deg	-25 to 25	0.5
Right throttle, percent	60 to 110	1.0
Left throttle, percent	60 to 110	1.0
Aileron trim tab, deg	-20 to 20	0.4
Elevator trim tab, deg	-20 to 20	0.4
Rudder trim, deg	-22 to 7	0.3

TABLE 3. — VARIATION OF MOMENTS OF INERTIA WITH WING SWEEP

[Values include pilot, gear, and full fuel; gross weight = 9540 N (2145 lb)]

Wing sweep, deg	I_x, kg-m^2 (slug-ft^2)	I_y, kg-m^2 (slug-ft^2)	I_z, kg-m^2 (slug-ft^2)	I_{xy}, kg-m^2 (slug-ft^2)	I_{xz}, kg-m^2 (slug-ft^2)
0	922.8 (680.6)	3239 (2389)	4088 (3015)	0 (0)	72.5 (53.5)
15	878.0 (647.6)	3284 (2422)	4088 (3015)	167.2 (123.2)	72.8 (53.7)
30	755.6 (557.3)	3406 (2512)	4088 (3015)	289.6 (213.6)	73.8 (54.4)
45	588.3 (433.9)	3573 (2635)	4088 (3015)	335.7 (246.7)	75.1 (55.4)
60	421.1 (310.6)	3741 (2759)	4088 (3015)	289.6 (213.6)	77.0 (56.8)

TABLE 4. — MAXIMUM CRAMER-RAO BOUNDS FOR PLOTTED DATA

[Values include scale factor of 2]

Derivative	Bound, ±
C_{m_α}, deg^{-1}	0.0018
C_{m_q}, rad^{-1}	5.0
$C_{m_{\delta_e}}$, deg^{-1}	0.002
C_{ℓ_β}, deg^{-1}	0.0001
C_{n_β}, deg^{-1}	0.0001
C_{Y_β}, deg^{-1}	0.0015
$C_{\ell_{\delta_a}}$, deg^{-1}	0.0001
$C_{n_{\delta_a}}$, deg^{-1}	0.0001
$C_{Y_{\delta_a}}$, deg^{-1}	0.00045

Derivative	Bound, ±
$C_{\ell_{\delta_r}}$, deg^{-1}	0.00003
$C_{n_{\delta_r}}$, deg^{-1}	0.00002
$C_{Y_{\delta_r}}$, deg^{-1}	0.0003
C_{ℓ_q}, rad^{-1}	1.0
C_{ℓ_p}, rad^{-1}	0.03
C_{ℓ_r}, rad^{-1}	0.05
C_{n_q}, rad^{-1}	0.4
C_{n_p}, rad^{-1}	0.03
C_{n_r}, rad^{-1}	0.03

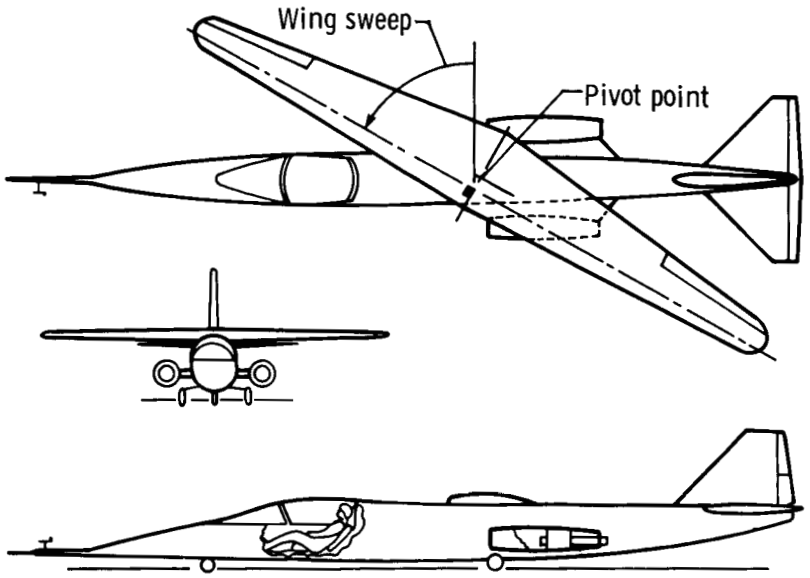

Figure 1. AD-1 general configuration.

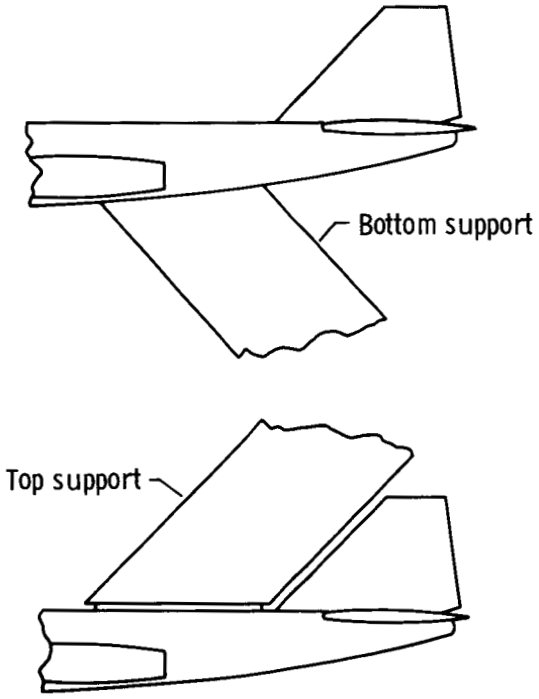

Figure 2. Wind tunnel model blade support arrangements.

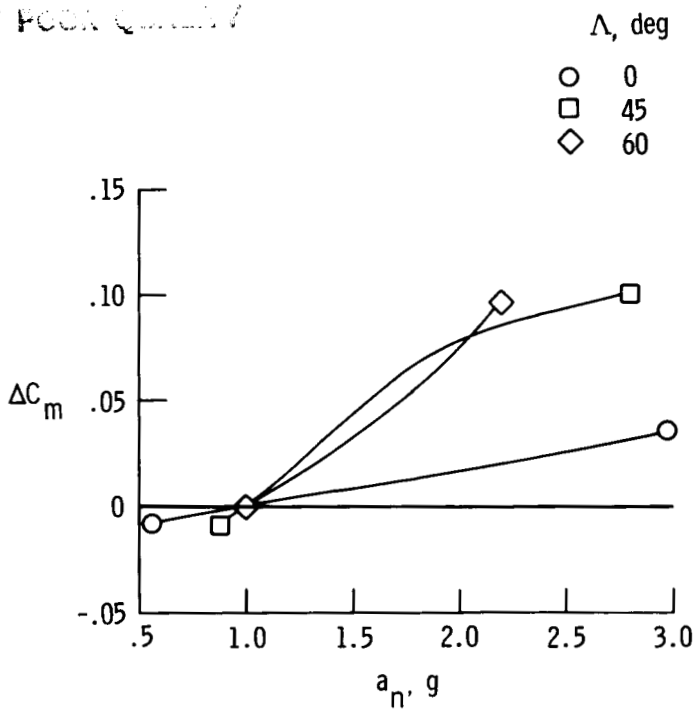

Figure 3. Flight-determined change in pitching moment due to load factor (from ref. 4). Controls zeroed, cg = 0.4c_r.

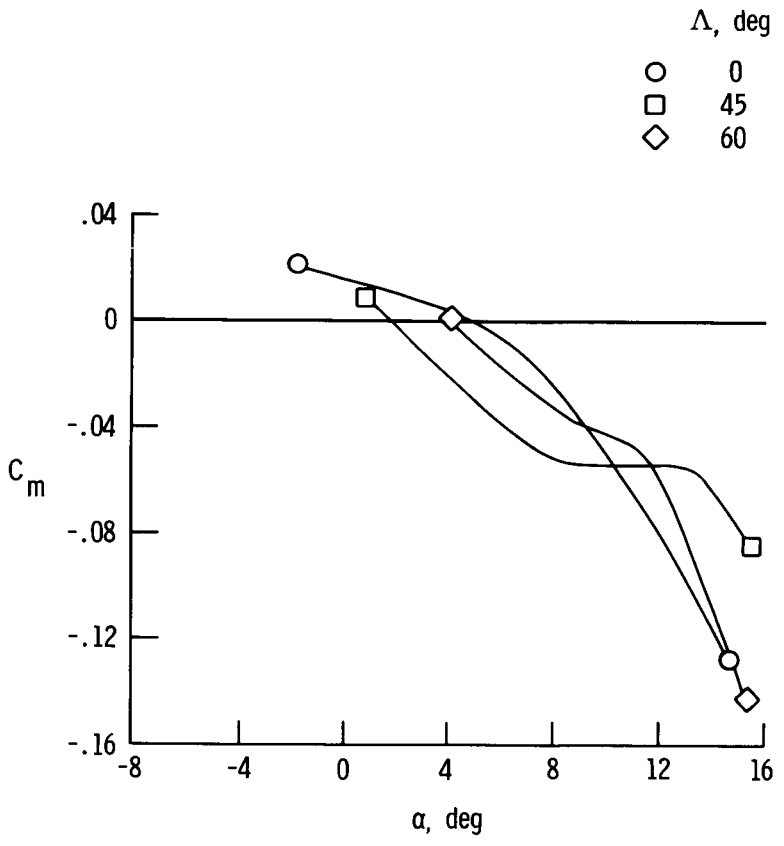

Figure 4. Pitching moment as a function of angle of attack for 1g flight (from ref. 4). Controls zeroed, cg = 0.4c_r.

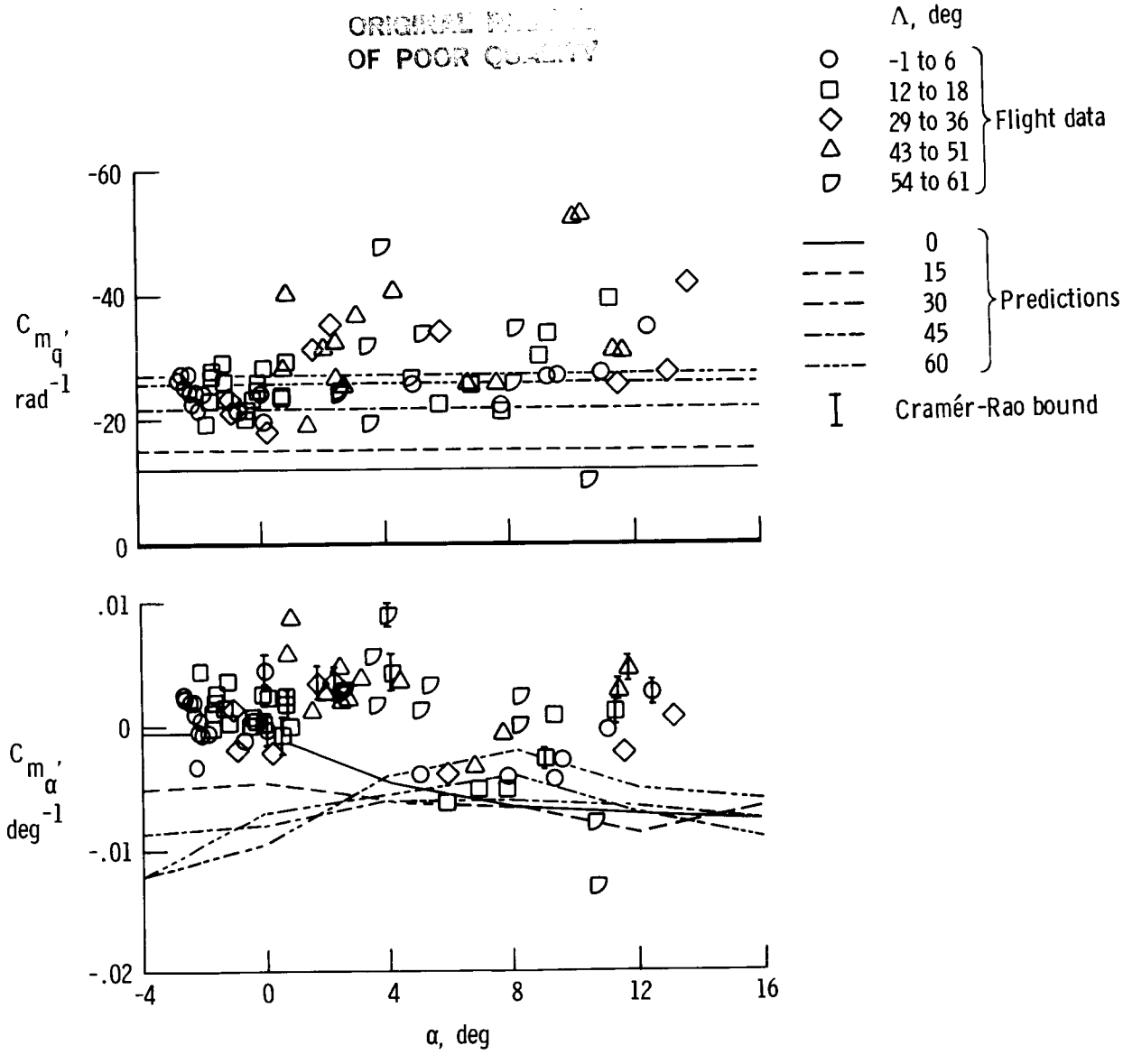

Figure 5. An example of C_{m_α} and C_{m_q} as obtained from MMLE3 analysis.

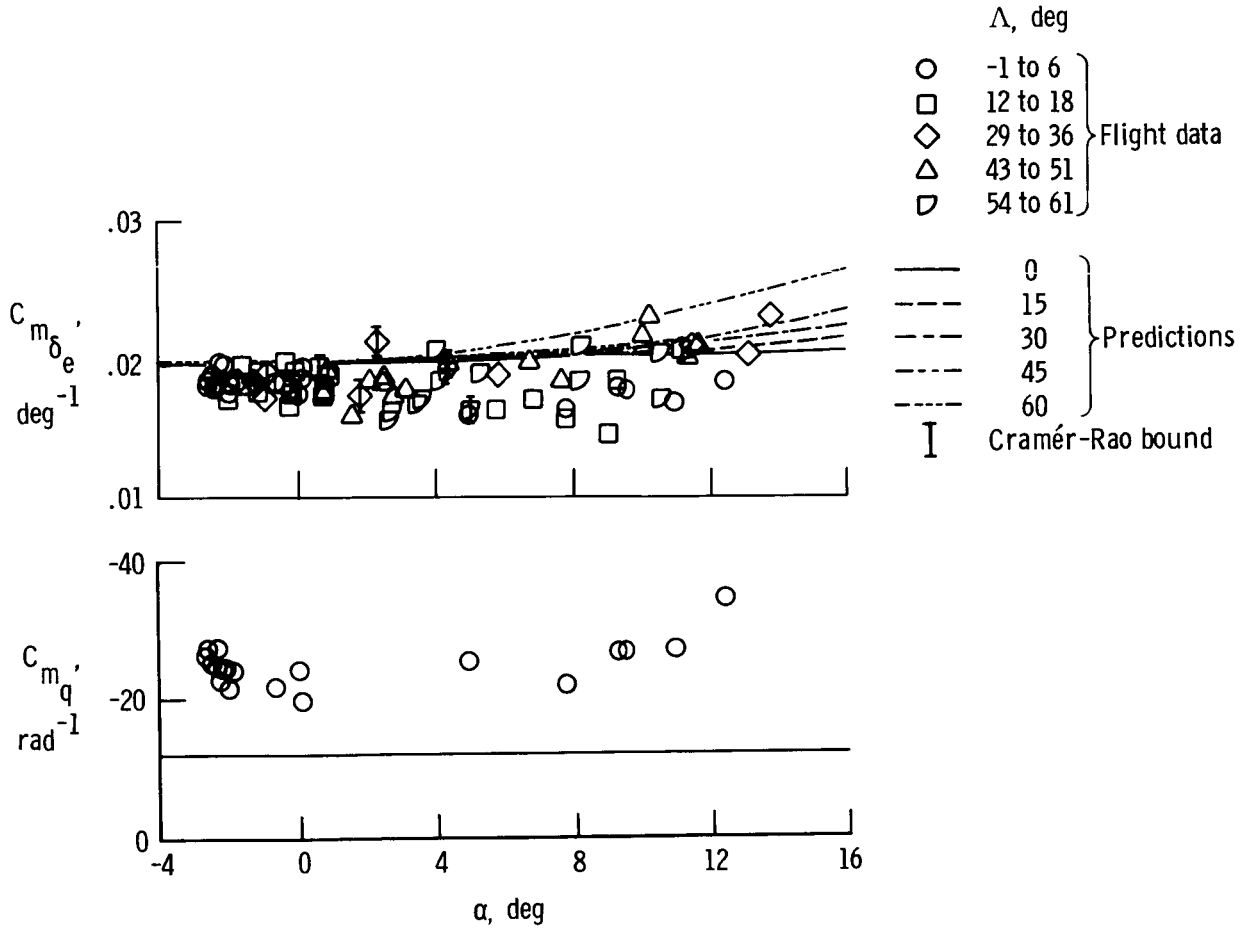

Figure 6. Estimates of $C_{m_{\delta_e}}$ and C_{m_q}.

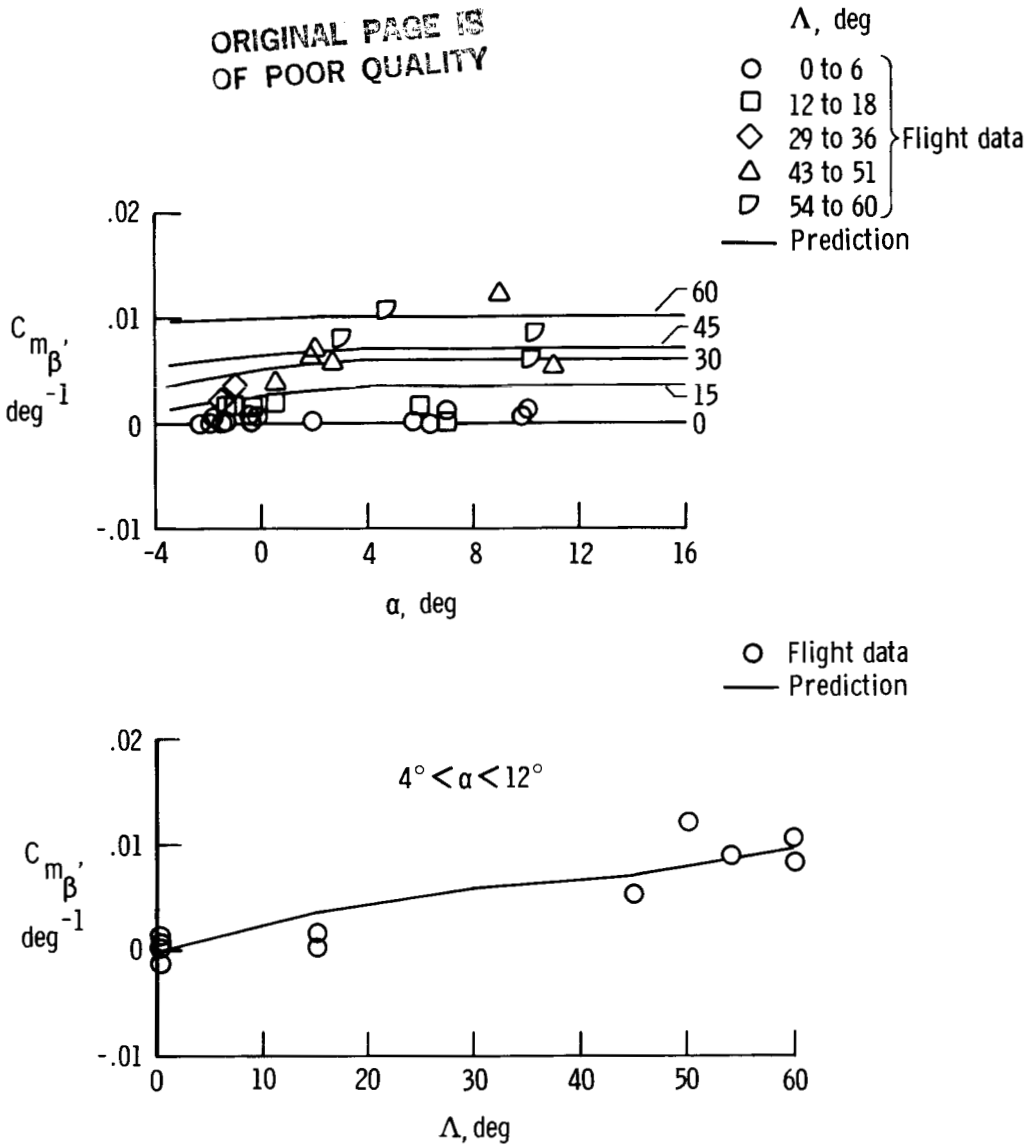

Figure 7. Estimates of C_{m_β} as obtained from sideslip variation analysis.

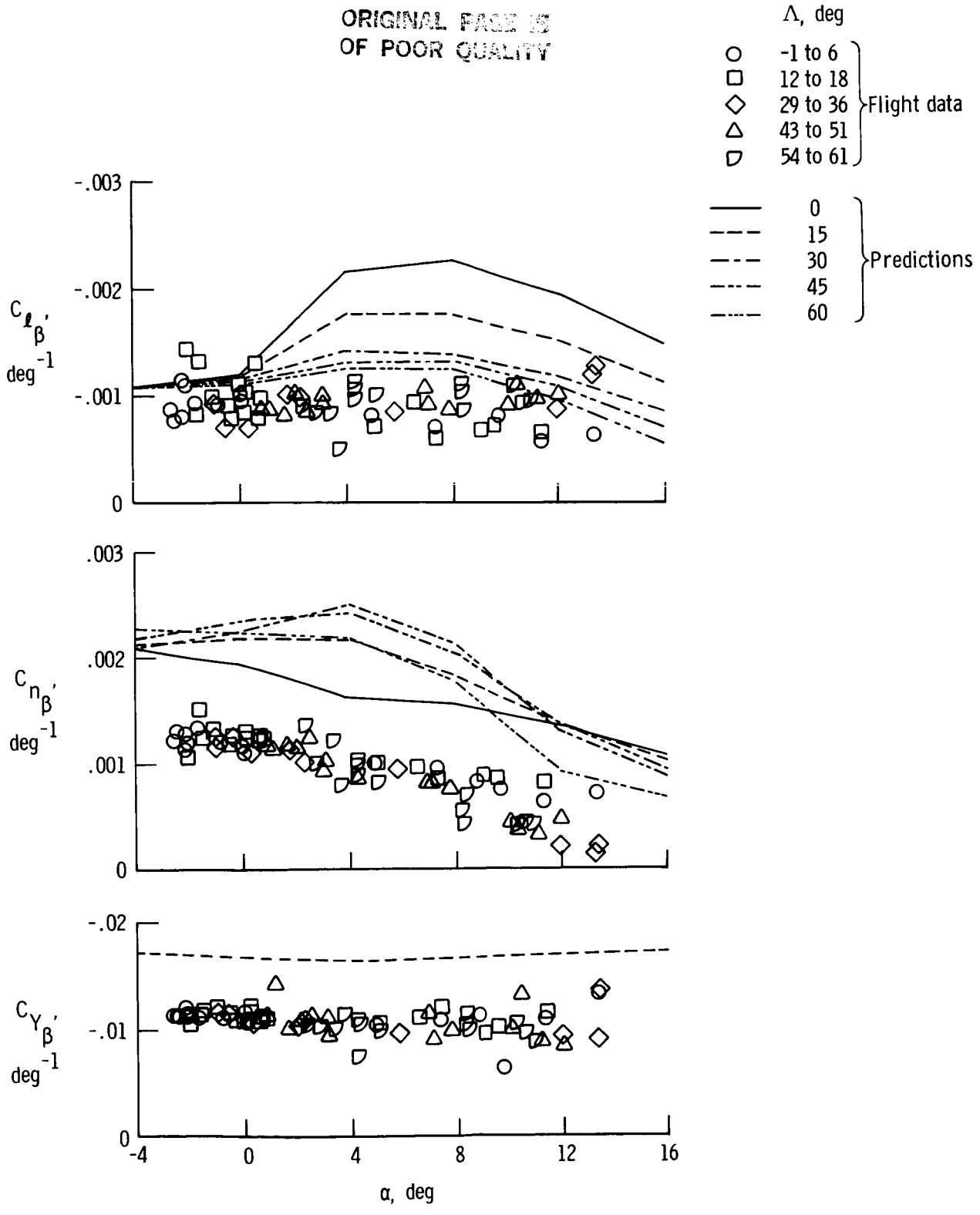

Figure 8. Estimates of C_{ℓ_β}, C_{n_β}, and C_{Y_β} as obtained from MMLE3 analysis.

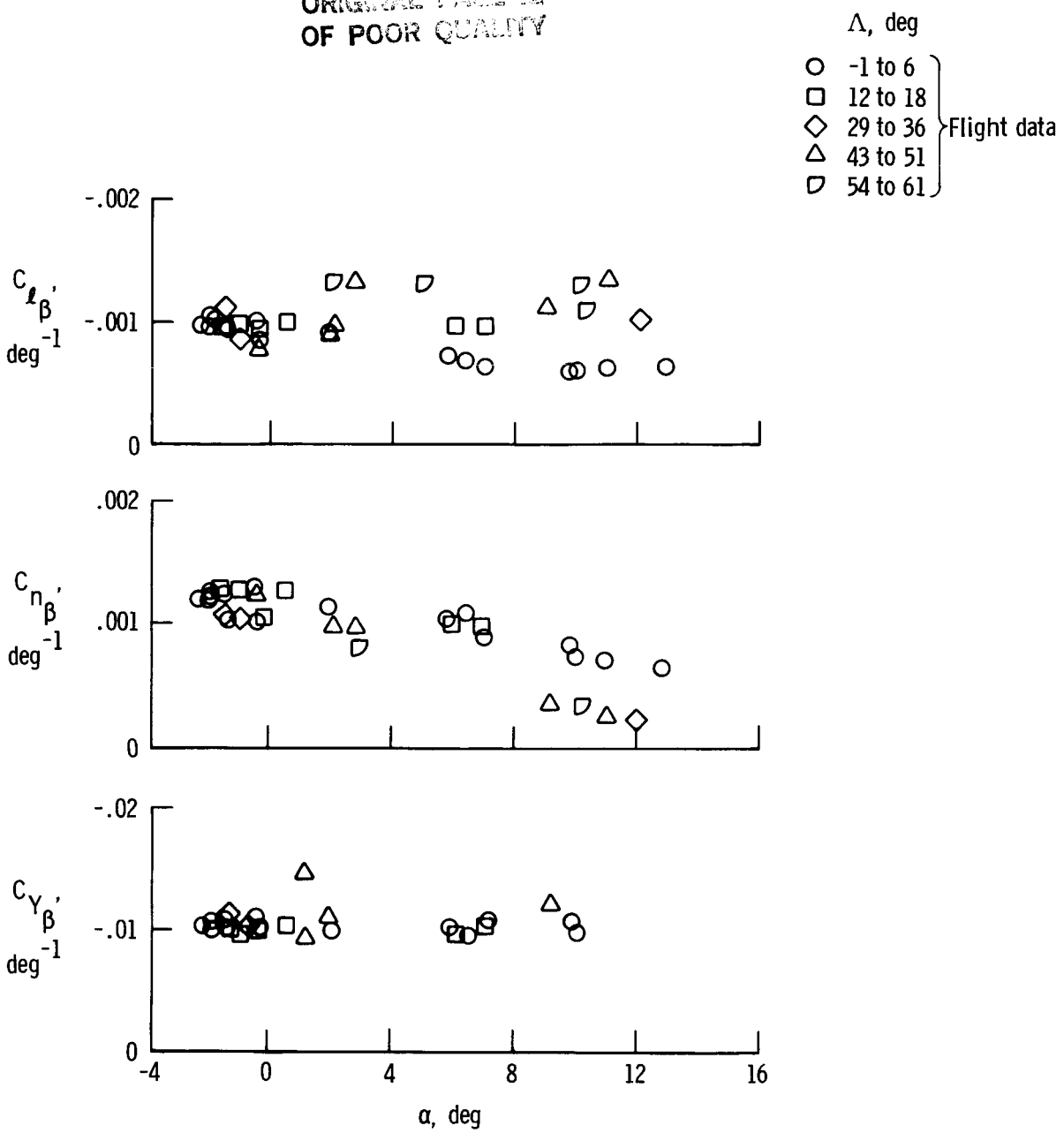

Figure 9. Estimates of C_{ℓ_β}, C_{n_β}, and C_{Y_β} as obtained from sideslip variation analysis.

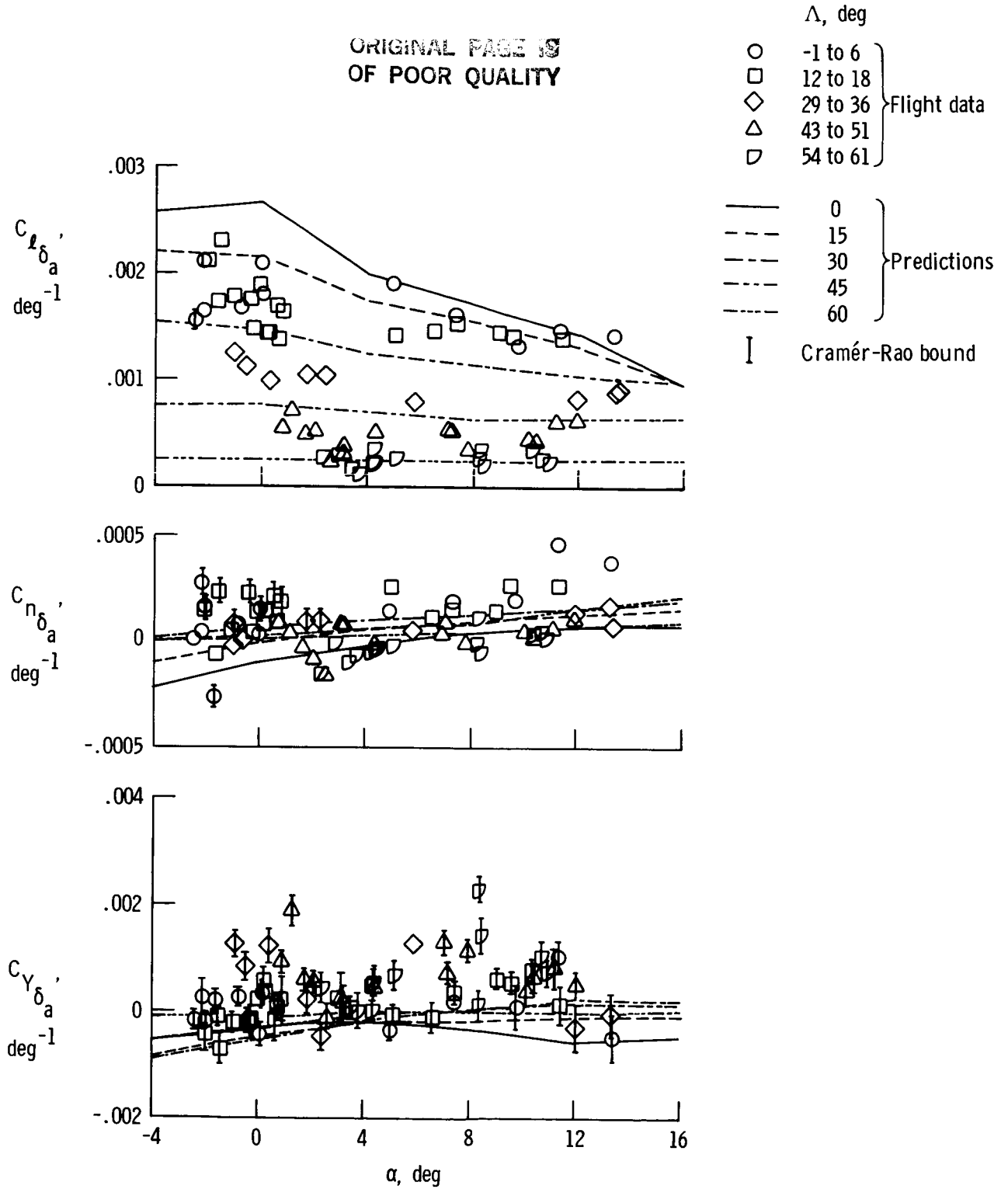

Figure 10. Estimates of $C_{\ell_{\delta_a}}$, $C_{n_{\delta_a}}$, and $C_{Y_{\delta_a}}$ as functions of angle of attack.

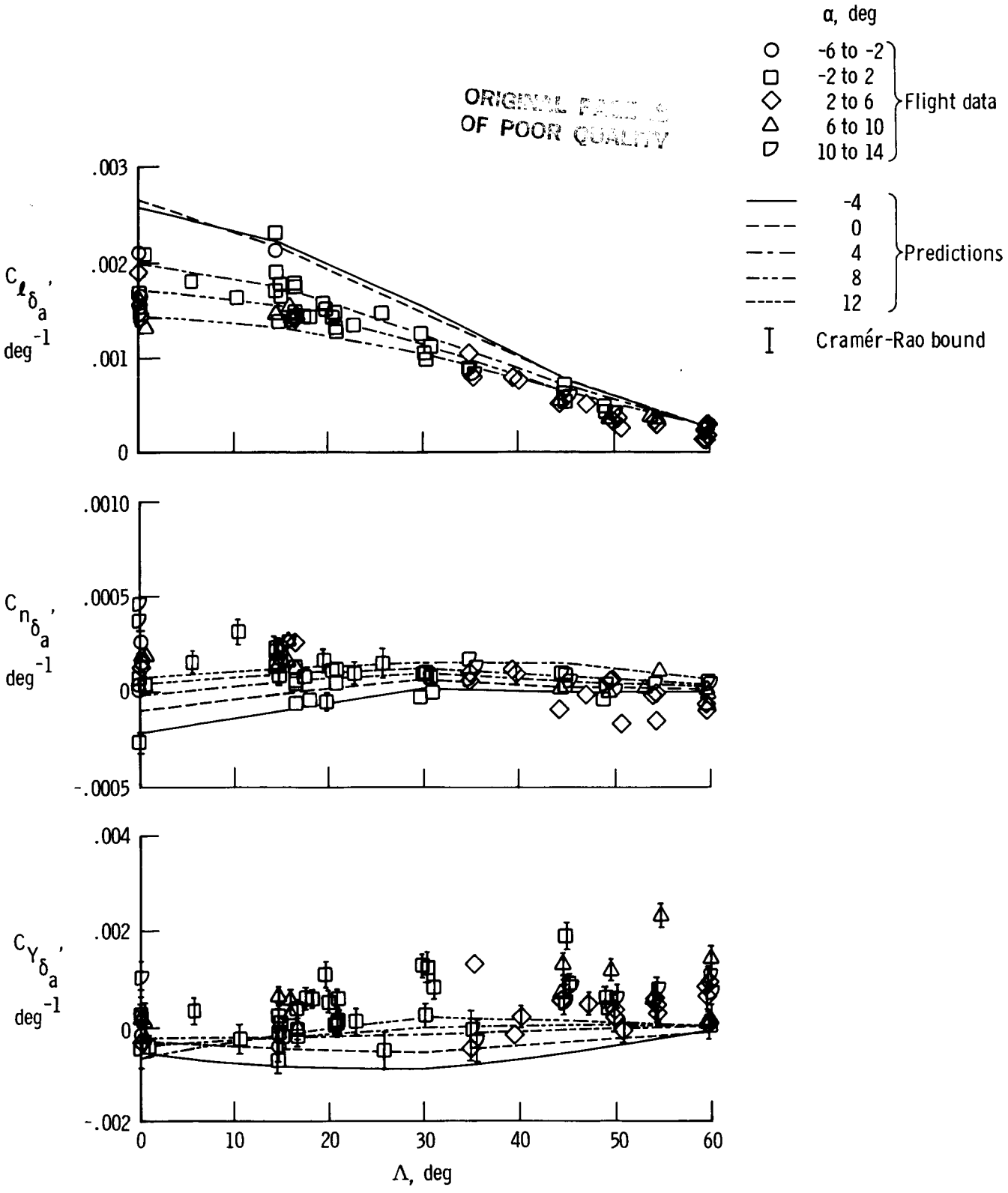

Figure 11. Estimates of $C_{\ell_{\delta_a}}$, $C_{n_{\delta_a}}$, and $C_{Y_{\delta_a}}$ as functions of wing sweep.

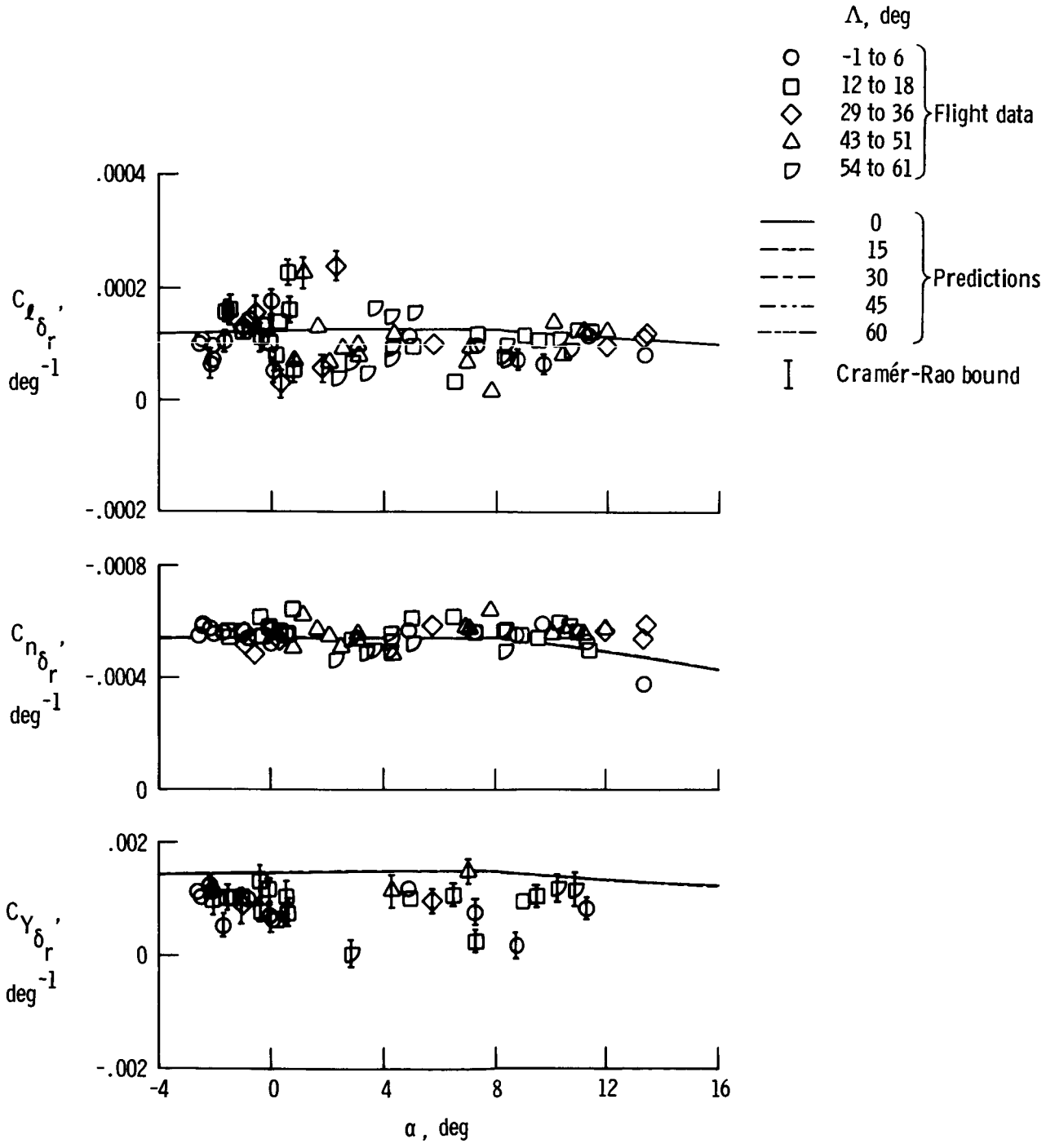

Figure 12. Estimates of $C_{\ell_{\delta_r}}$, $C_{n_{\delta_r}}$, and $C_{Y_{\delta_r}}$ as functions of angle of attack.

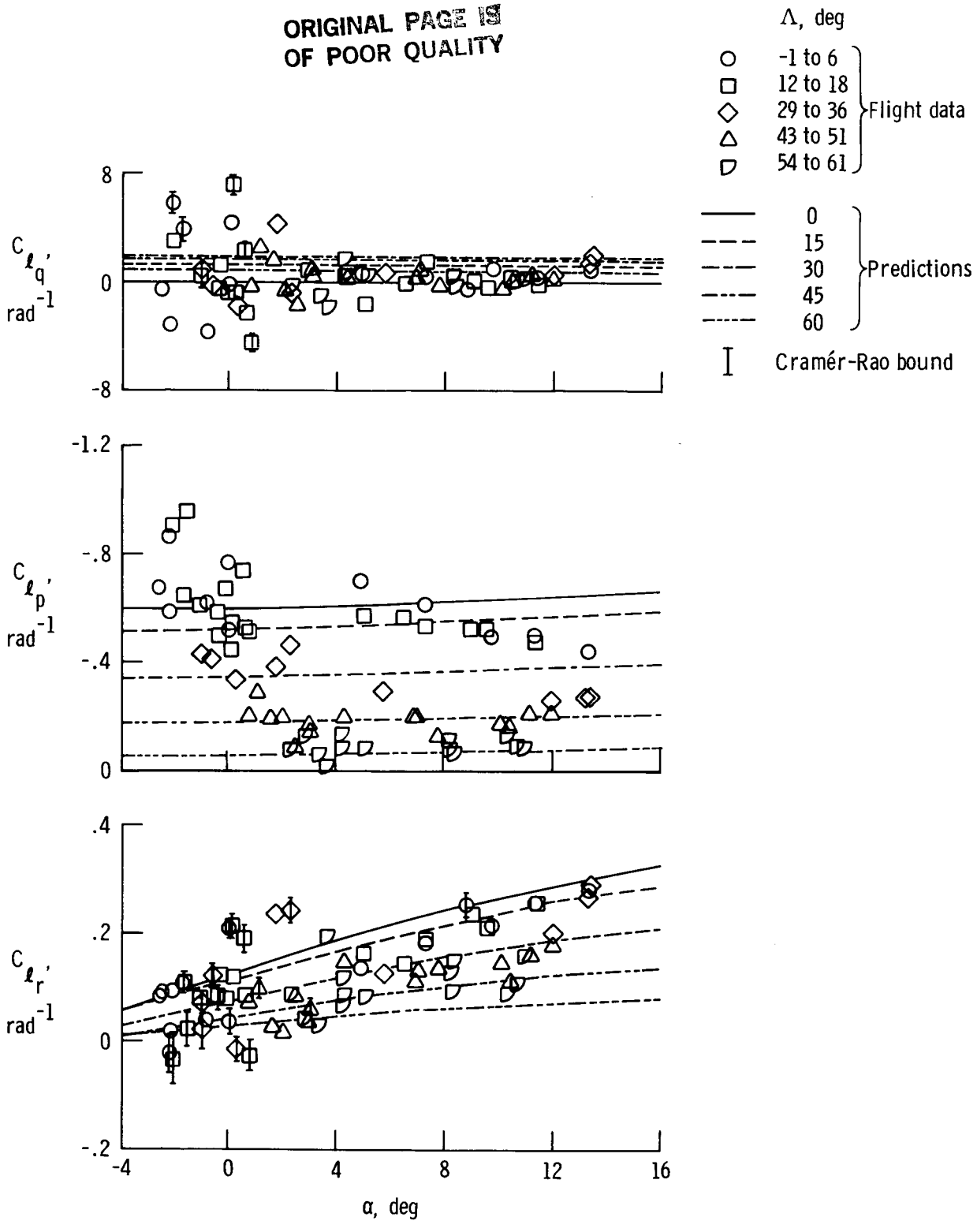

Figure 13. Estimates of C_{ℓ_q}, C_{ℓ_p}, and C_{ℓ_r} as functions of angle of attack.

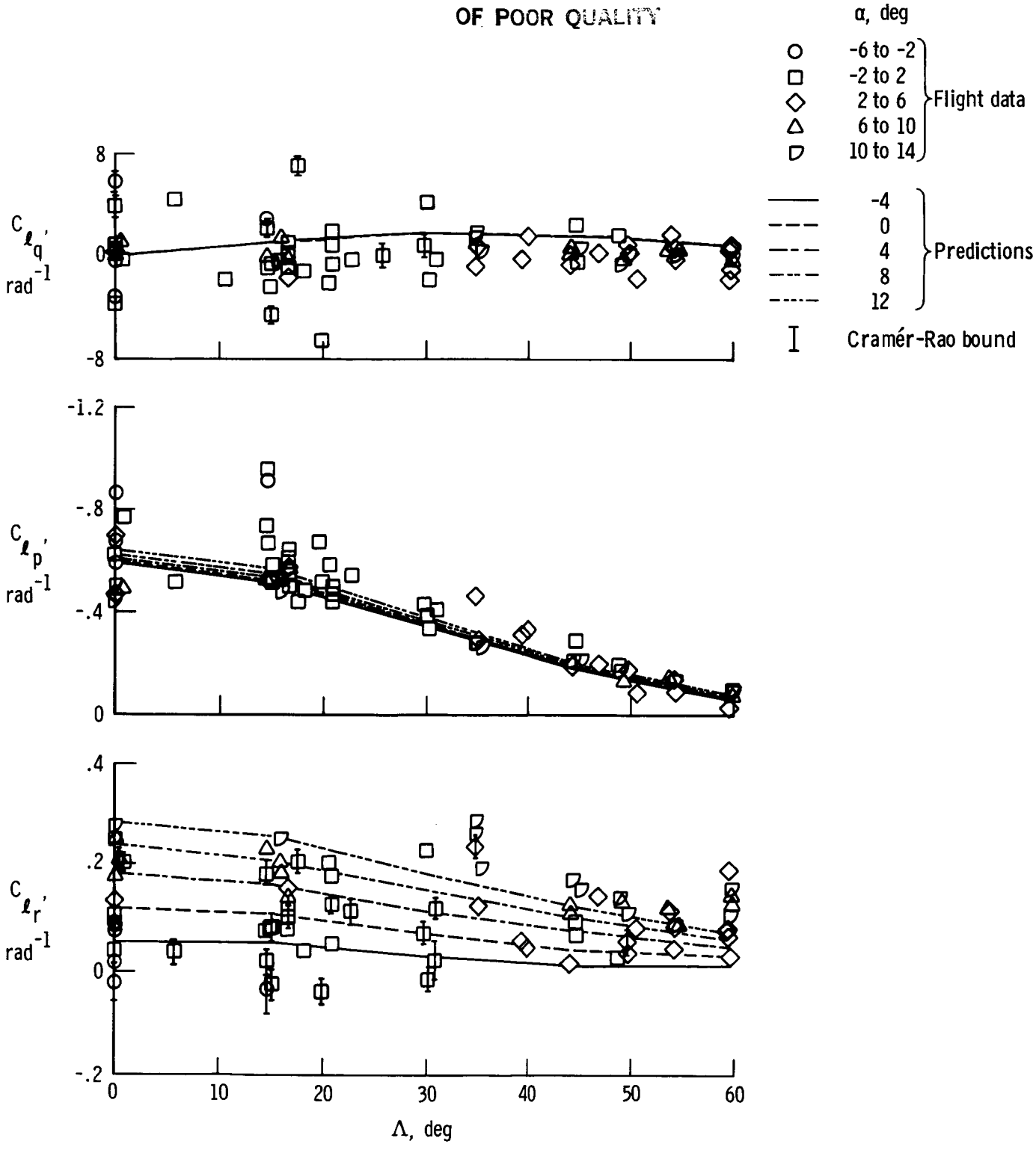

Figure 14. Estimates of C_{ℓ_q}, C_{ℓ_p}, and C_{ℓ_r} as functions of wing sweep.

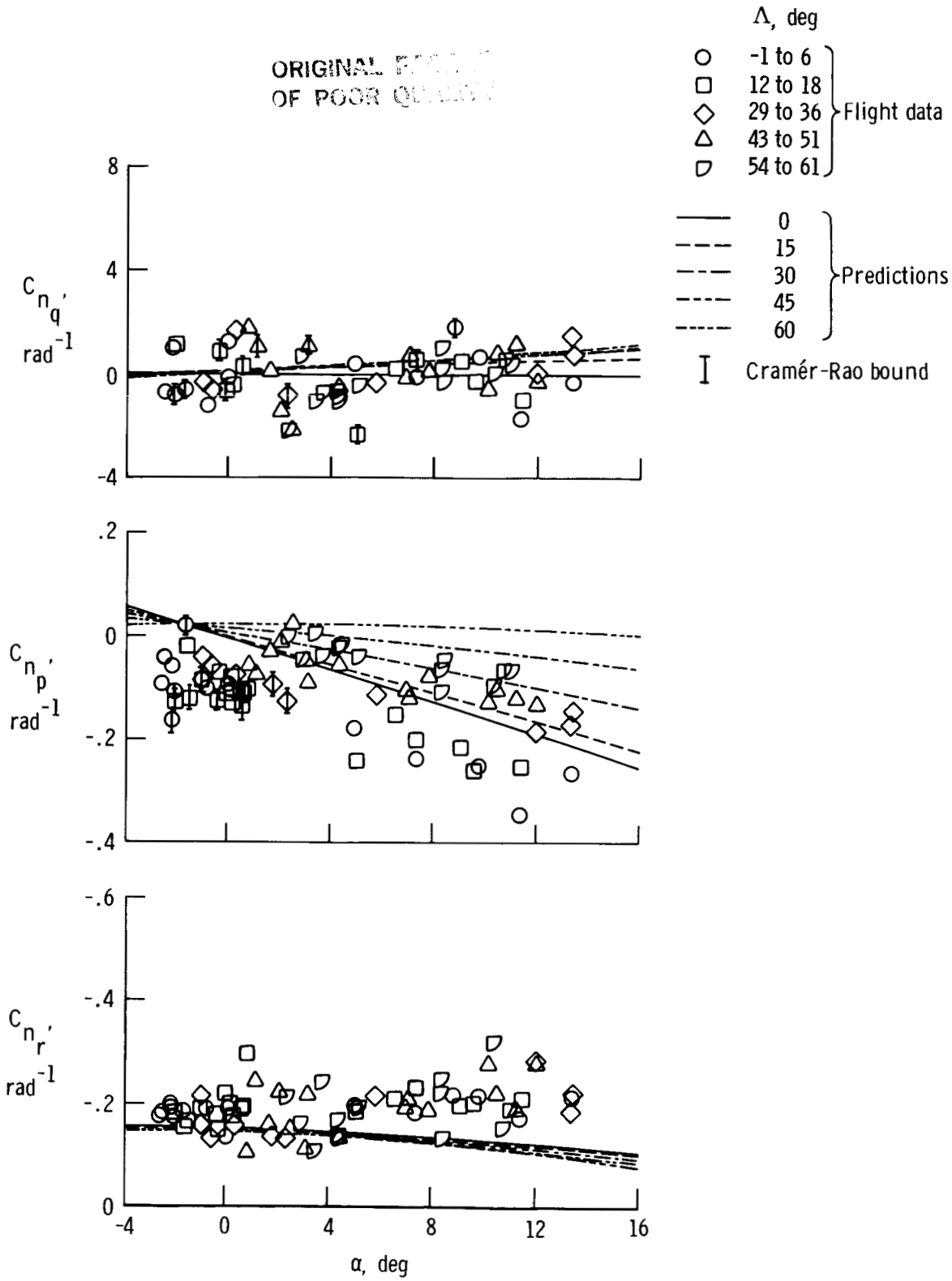

Figure 15. Estimates of C_{n_q}, C_{n_p}, and C_{n_r} as functions of angle of attack.

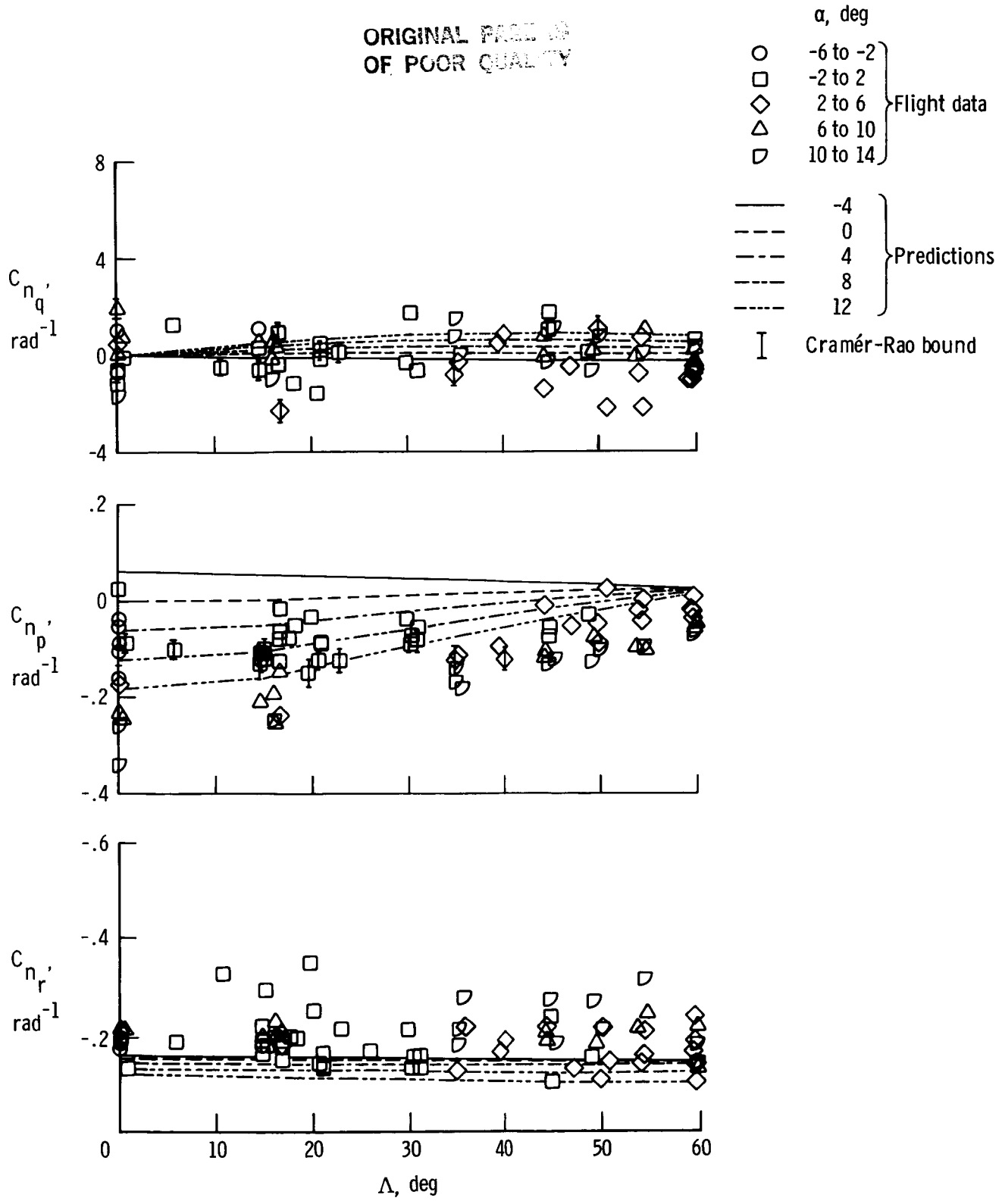

Figure 16. Estimates of C_{n_q}, C_{n_p}, and C_{n_r} as functions of wing sweep.

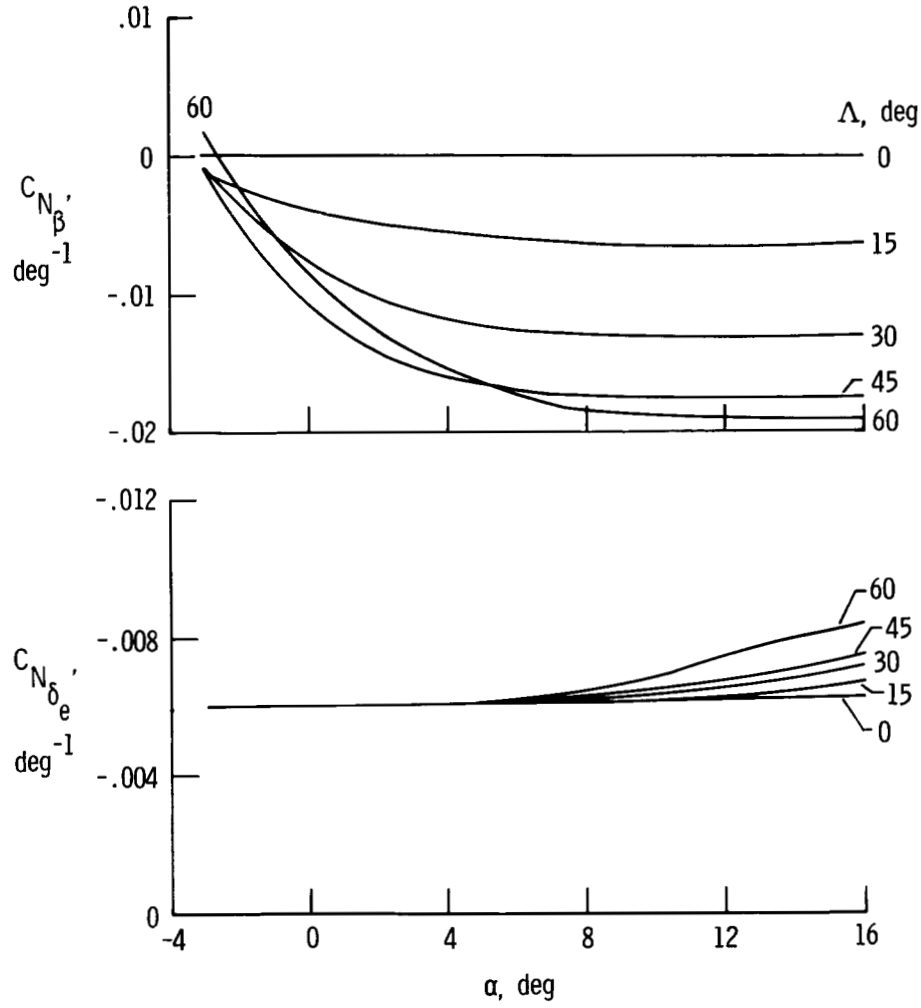

(a) $C_{N\beta}$ and $C_{N\delta_e}$.

Figure 17. Best estimate of longitudinal derivatives.

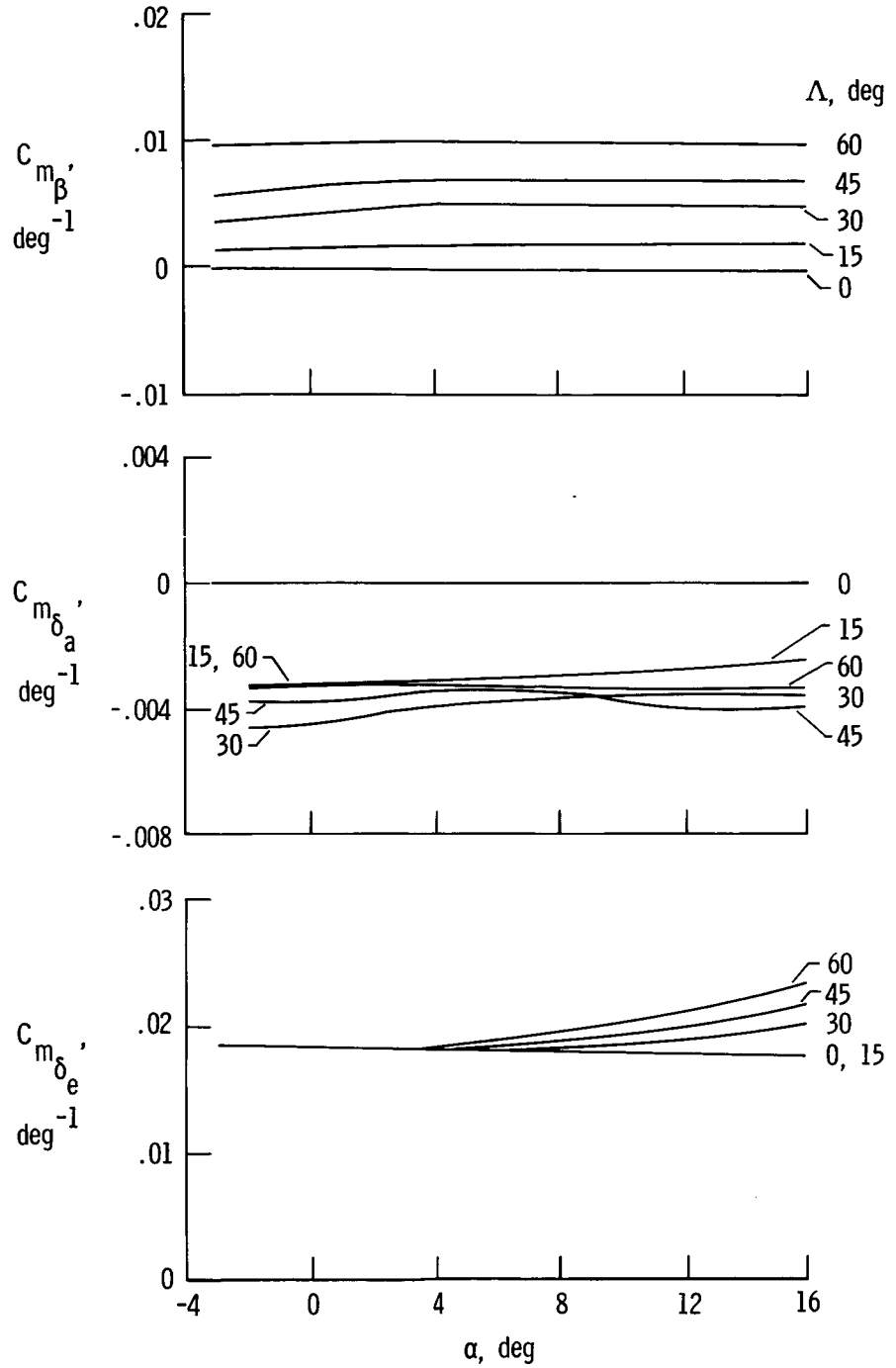

(b) C_{m_β}, $C_{m_{\delta_a}}$, *and* $C_{m_{\delta_e}}$.

Figure 17. Continued.

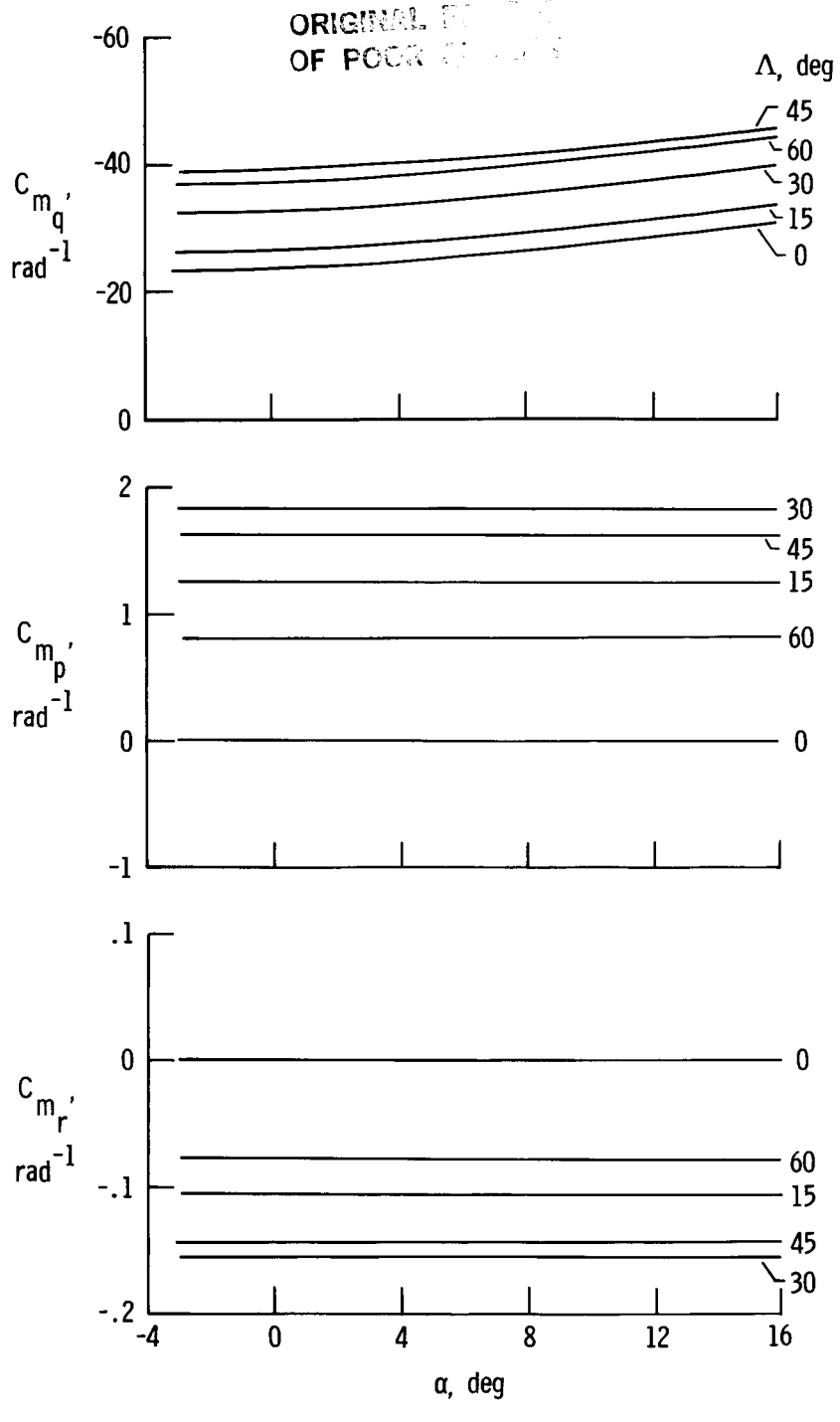

(c) C_{m_q}, C_{m_p}, and C_{m_r}.

Figure 17. Concluded.

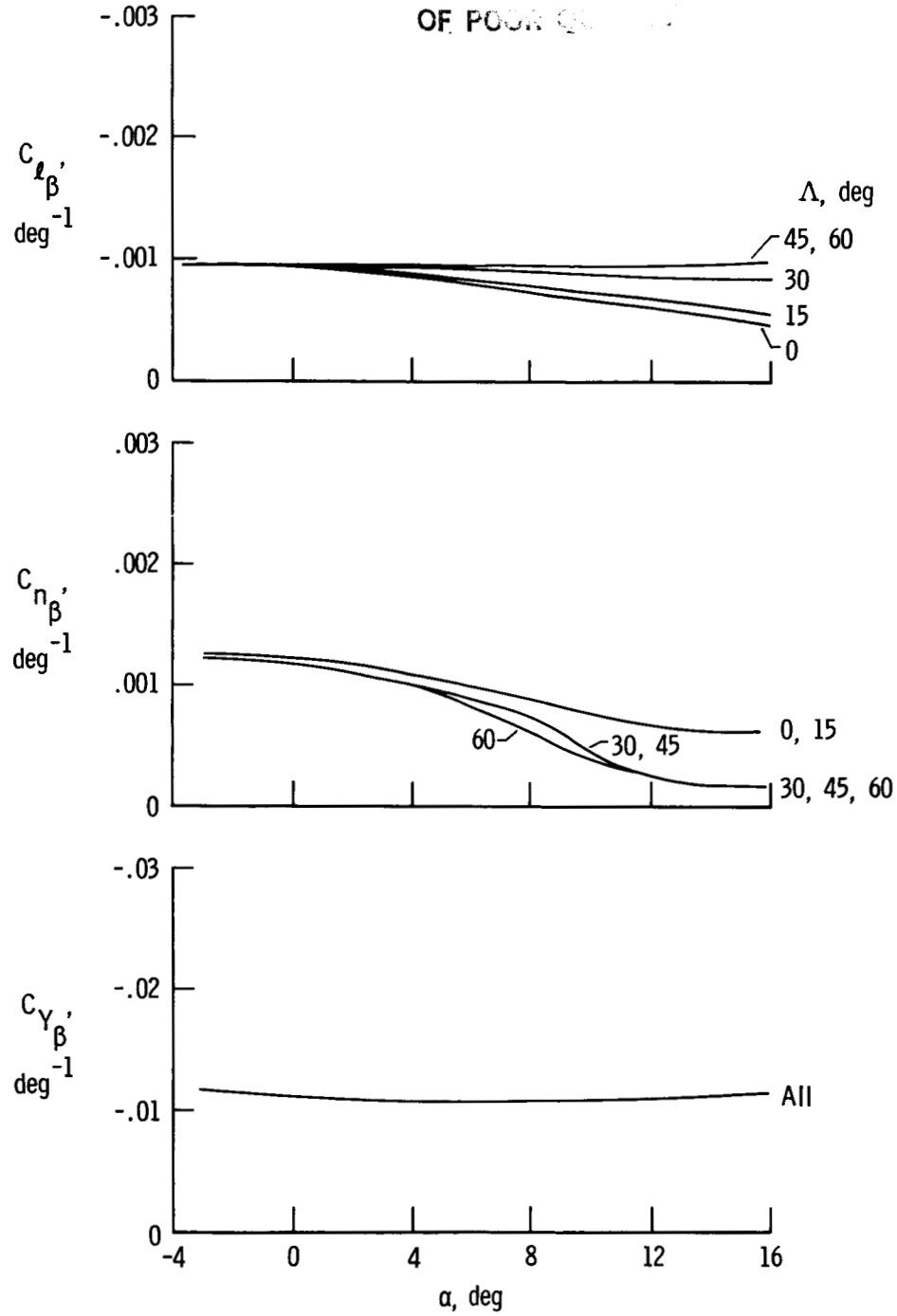

(a) C_{ℓ_β}, C_{n_β}, and C_{Y_β}.

Figure 18. Best estimate of lateral-directional derivatives.

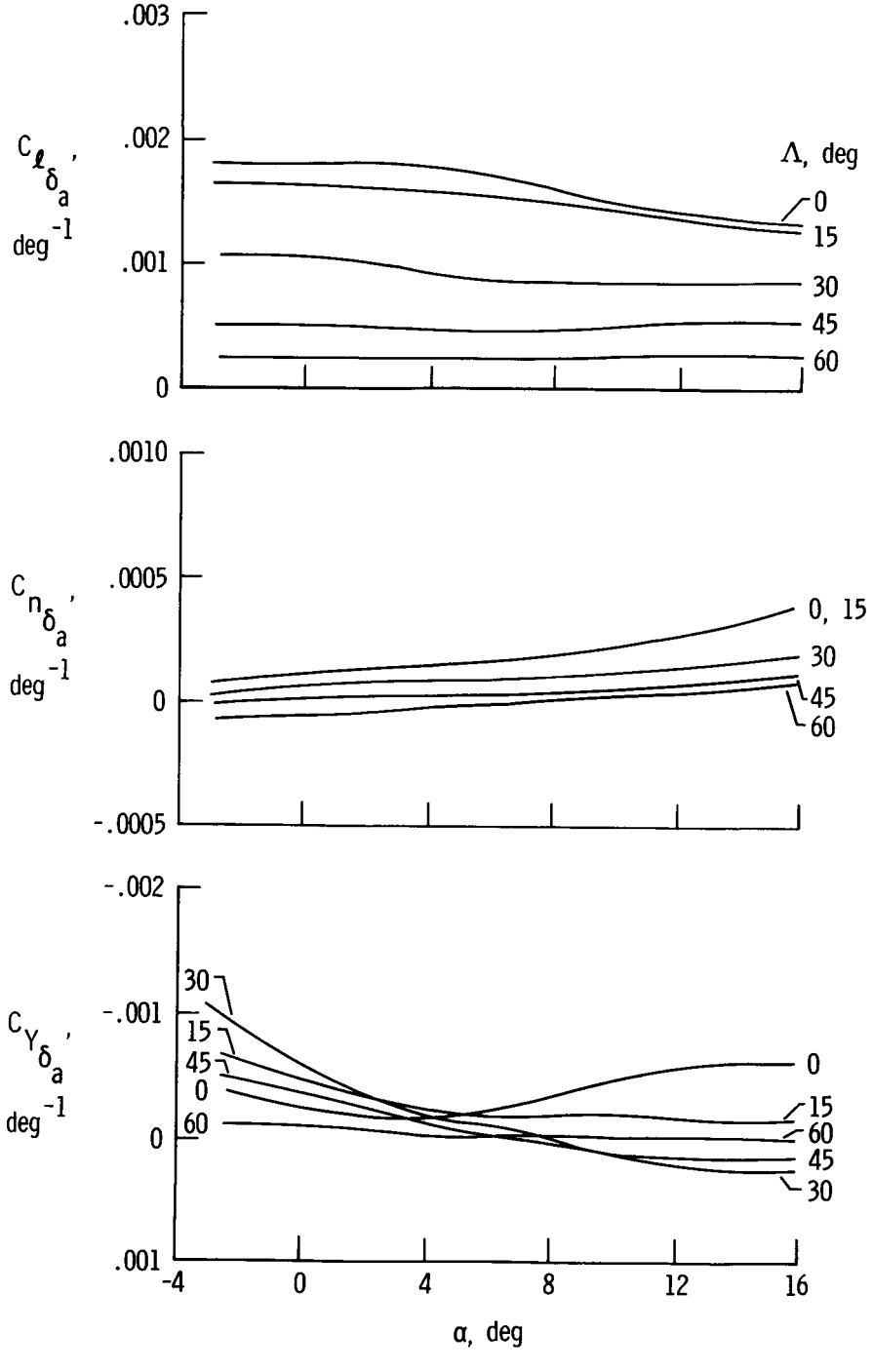

(b) $C_{\ell_{\delta_a}}$, $C_{n_{\delta_a}}$, *and* $C_{Y_{\delta_a}}$.

Figure 18. Continued.

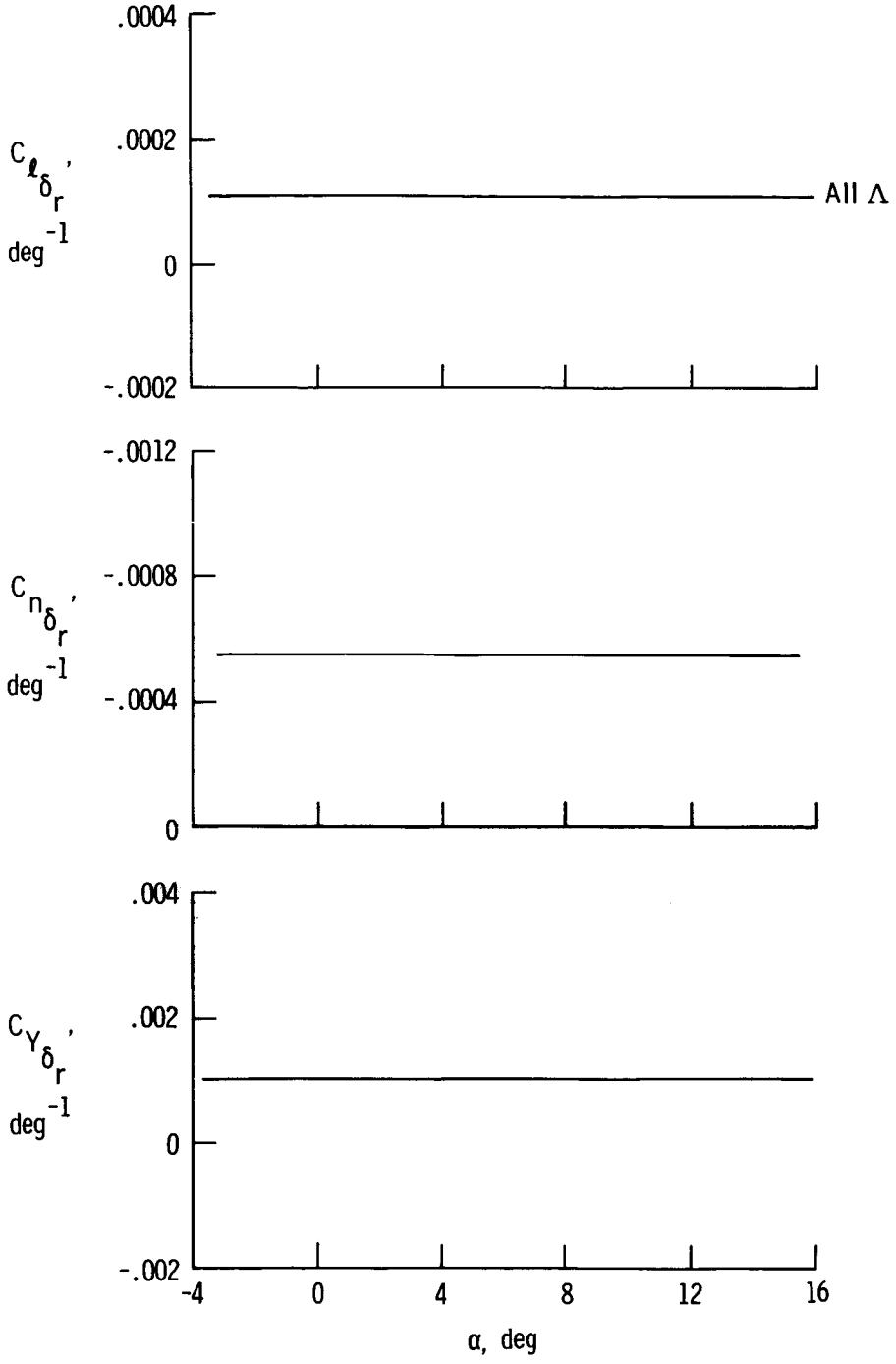

(c) $C_{\ell_{\delta_r}}$, $C_{n_{\delta_r}}$, and $C_{Y_{\delta_r}}$.

Figure 18. Continued.

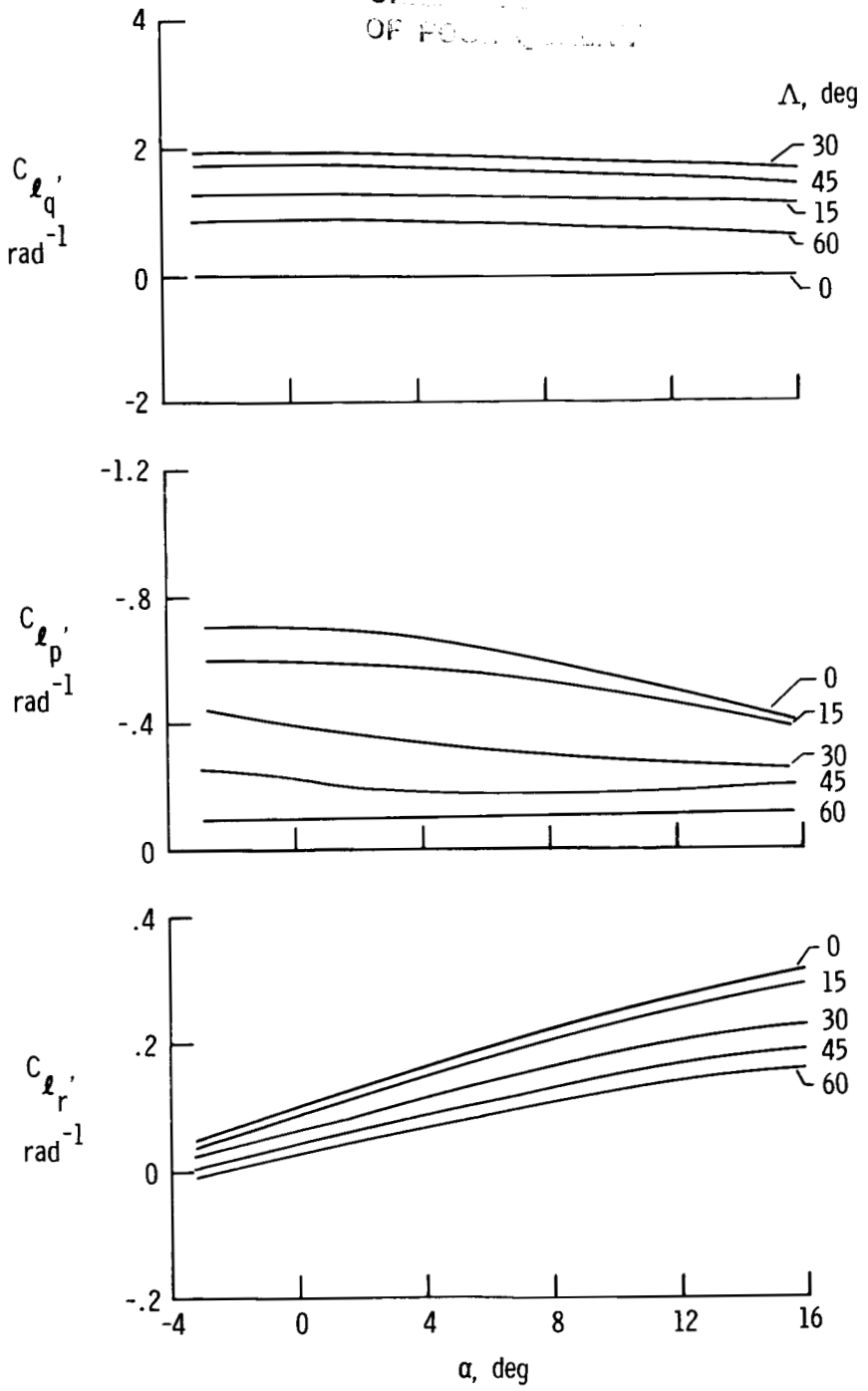

(d) C_{ℓ_q}, C_{ℓ_p}, and C_{ℓ_r}.

Figure 18. Continued.

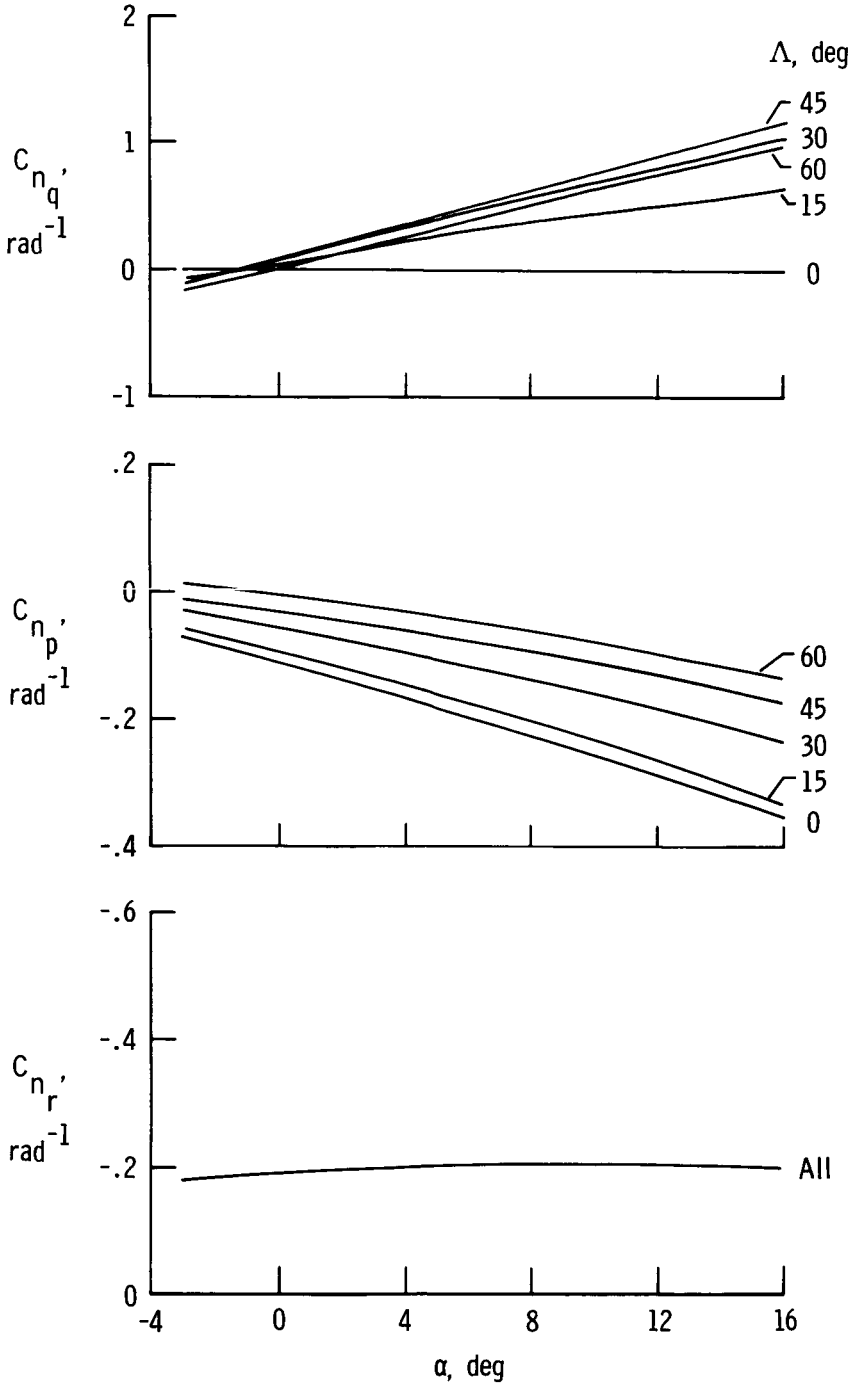

(e) C_{n_q}, C_{n_p}, and C_{n_r}.

Figure 18. Concluded.

1. Report No.	2. Government Accession No.	3. Recipient's Catalog No.
NASA TP-2222		

4. Title and Subtitle	5. Report Date
Flight-Determined Aerodynamic Derivatives of the AD-1 Oblique-Wing Research Airplane	October 1984
	6. Performing Organization Code

7. Author(s)	8. Performing Organization Report No.
Alex G. Sim and Robert E. Curry	H-1179
	10. Work Unit No.

9. Performing Organization Name and Address	11. Contract or Grant No.
NASA Ames Research Center Dryden Flight Research Facility P.O. Box 273 Edwards, California 93523	
	13. Type of Report and Period Covered
12. Sponsoring Agency Name and Address	Technical Paper
National Aeronautics and Space Administration Washington, D.C. 20546	14. Sponsoring Agency Code
	RTOP 505-43-44

15. Supplementary Notes

16. Abstract

The AD-1 is a variable-sweep oblique-wing research airplane that exhibits unconventional stability and control characteristics. In this report, flight-determined and predicted stability and control derivatives for the AD-1 airplane are compared. The predictions are based on both wind tunnel and computational results. A final "best estimate" of derivatives is presented.

17. Key Words (Suggested by Author(s))	18. Distribution Statement
AD-1 aircraft Oblique wing Derivatives Parameter identification Stability and control	[redacted]

19. Security Classif. (of this report)	20. Security Classif. (of this page)	21. No. of Pages	22. Price
Unclassified	Unclassified	40	

[redacted]

NASA-Langley, 1984